# Electromigration and stress-induced voiding in fine Al and Al-alloy thin-film lines

by C.-K. Hu K. P. Rodbell T. D. Sullivan

K. Y. Lee

D. P. Bouldin

Physical phenomena underlying failure due to electromigration and stress-induced voiding in fine AI and AI-alloy thin-film conducting lines are examined in the context of accelerated testing methods and structures. Aspects examined include effects due to line isolation (the absence of reservoirs at conductor ends), solute and precipitate phenomena, conductor critical (Blech) length, microstructure, film deposition conditions, and thermal processing subsequent to film deposition. Emphasis is on the isolated, submicron-wide, AI(Cu)-based thin-film interconnection lines of IBM VLSI logic and memory chips.

# Introduction

The on-chip interconnections of IBM VLSI logic and memory chips contain up to five levels of isolated Al(Cu)-based thin-film lines having widths down to 0.5  $\mu$ m, and associated tungsten via connections [1]. Reliability targets require that far less than one chip per thousand should experience an interconnection or "wiring" failure during years of field operation. We focus on failure mechanisms due to electromigration (EM) [2] and mechanical-stress-induced voiding (SV) (commonly referred to as stress

migration) [3]. Both are of critical importance at current VLSI and forthcoming ULSI levels of integration. They involve the gradual formation of voids in the fine, thin-film lines or "wires" used for circuit interconnection, eventually causing circuit wiring failures due to the associated development of resistance increases, electrical opens, or (indirectly) electrical shorts. The primary driving force for EM is the electric current that is carried in the wires; for SV it is the thermal expansion mismatches between the wires and 1) the insulating layers [4] which enclose them and 2) the underlying silicon chip. The mass transport responsible for void formation and the nucleation points at which failures occur as the atoms in the wires respond to these forces can be significantly different for these two mechanisms.

Two key themes of this paper are the importance of understanding the dependence of accelerated testing data on the type of testing structures used—and the need to analyze those data not in terms of simple "time-to-fail" analysis, as is usually done, but rather in terms of resistance degradation as a function of time. The latter approach is preferred both because of the light it can shed on underlying failure mechanisms and because it permits more realistic projections of accelerated failure data to field conditions.

<sup>e</sup>Copyright 1995 by International Business Machines Corporation. Copying in printed form for private use is permitted without payment of royalty provided that (1) each reproduction is done without alteration and (2) the Journal reference and IBM copyright notice are included on the first page. The title and abstract, but no other portions, of this paper may be copied or distributed royalty free without further permission by computer-based and other information-service systems. Permission to republish any other portion of this paper must be obtained from the Editor.

0018-8646/95/\$3.00 © 1995 IBM

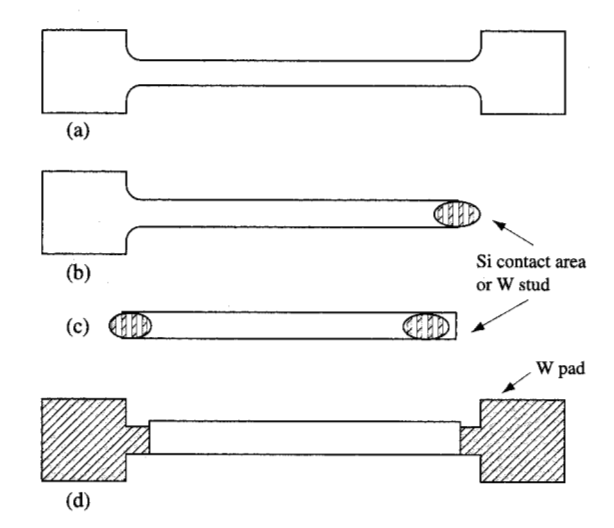


Figure 1

Accelerated test structures: (a) line with two reservoirs; (b) line with one reservoir; (c) and (d) lines without reservoirs.

EM and SV in Al-alloy films are each influenced by macrostructural factors such as the geometry of the test structures used to investigate them [5], materials selection [6], layering sequence [7], patterning dimensions [8, 9], topography [10], and interlayer connection methodology [11]. They are also influenced by microstructural aspects such as metal grain size and grain size distribution [12], crystallographic grain orientation (texture) [13], alloy solute distribution and precipitation [14], dislocation densities [15], and the number and quality of interfaces that may be present [16].

In IBM VLSI on-chip interconnections containing five levels of Al(Cu)-based lines, those of the first level are typically in contact with areas in the underlying silicon, polysilicon gate conductors, (short) tungsten lines, and tungsten posts or "studs"; those of the second, third, and fourth levels are in contact with each other and with lines of the first level through interlevel tungsten studs; and those of the fifth level are in direct contact with the lines of the fourth level and overlying solder terminals.

Typically, the Al(Cu)-based lines are Ti/Al(0.5 wt.% Cu)/Ti/TiN lines. The (relatively thin) TiN layer is used to facilitate photoprocessing. The lines of the fifth level do not contain the uppermost Ti and TiN layers. In the course of subsequent thermal processing, the Ti layers react with the Al to form TiAl<sub>3</sub>. The lines of the fifth level are connected to lines of the fourth level through tapered via holes (tapering prevents significant thinning, which occurs

when contact through vertical vias is attempted). Although the contact portions of the TiAl<sub>3</sub> overlying the lines of the fourth level may be etched away during the formation of contacts between its lines and those of the fifth level, line isolation is maintained because of the presence of the TiAl<sub>3</sub> underlying the lines of the fifth level. Thus, the Al(Cu) portions of all the lines are physically isolated by tungsten studs and/or regions of TiAl<sub>3</sub>. That isolation has critical implications for EM and SV failure mechanisms and has often been overlooked.

Reliability with regard to EM and SV is typically evaluated by accelerated testing of simplified (compared to product designs) test structures. Acceleration is achieved by testing at higher-than-use temperatures. In the case of EM, additional acceleration is achieved by testing at higher-than-use current densities. Activation energies and other parameters derived from results obtained at different temperatures and current densities, respectively, are then used to develop projections to field conditions [17].

Four types of test structures discussed in this paper are shown in **Figure 1**. The double-reservoir, single-level structure shown in Figure 1(a) [18] is used in most EM and SV work reported in the literature. However, the majority of lines in current VLSI chips are more accurately represented by the single-reservoir, multilevel structure of Figure 1(b) [19] and/or the isolated or "closed" multilevel structures of Figures 1(c) [20] and 1(d) [21]. The latter is a variation of Figure 1(c), permitting the study of key aspects of EM failure with samples that can be more easily fabricated.

# Microstructural features

Microstructural features of metallic thin films, such as their median grain size, grain size distribution, crystallographic texture, and precipitate size and distribution, are all linked by kinetic parameters such as surface, interface, grain boundary, and bulk diffusivity. Although these kinetic parameters are intrinsic film parameters, their effects can be modified by controlling deposition processes and subsequent thermal annealing. The microstructural features of metallic thin films fabricated by physical vapor deposition depend mainly on the homologous deposition temperature  $(T/T_{\rm m}$ , where  $T_{\rm m}$  is the melting point of the film) and may be modified by controlling the cleanliness of the deposition and/or surface and with the use of thin seed layers [22]. However, grain size and film texture are often not controlled, which can lead to wide variations in the reliability of lines expected to be nominally identical.

# • Grain size

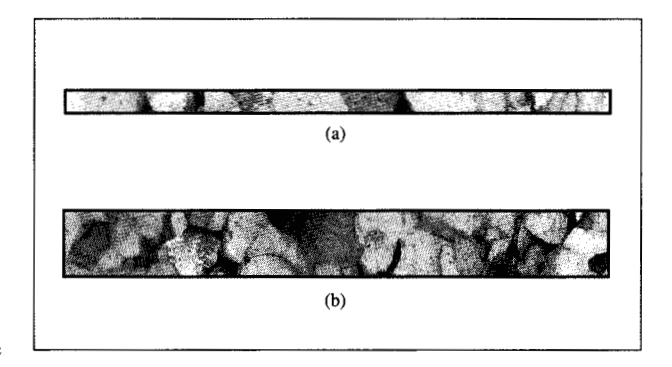
Median grain size is perhaps the most popular microstructural feature measured, both because it is conceptually appealing and because it is a well-known historical parameter in metallography. If the population follows a Gaussian distribution, it is simply the average grain size. For thin films, the population is often better described by a log-normal distribution, for which the median grain size is not the average grain size, but is often close to it. A property less popular than the median grain size, but probably more important to the reliability of metallic thin-film lines, is the spread (standard deviation) in grain sizes. If the spread is small (e.g., if the grain size distribution is narrow), the transport properties of such lines can be uniform along the line length and from line to line; if the spread is large (e.g., if there is a large difference in the length of polygrain segments), little uniformity in transport properties is likely.

The reason for grain size variation has been explored both theoretically and experimentally [23, 24], and is illustrated in the transmission electron micrographs (TEMs) in Figures 2(a) and 2(b). The wider line has a multigrain structure, in contrast to the narrower line, which exhibits a mostly single-grain-per-line-width or "bamboo-grained" structure. In the latter, nearly all of the grain boundaries are oriented normal to the major axis of the line. The bamboo structure often becomes dominant as the ratio of width to thickness of a well-annealed line approaches unity. In general, narrow lines are occasionally observed to have two grains across their width, while wide lines occasionally contain small sections of bamboo-type blocking grains. This dependence of structure upon line width can occur both with and without an underlayer [25], and is also found in Al(0.5-4 wt.% Cu) alloy lines [26]. This difference in grain structure from narrow to wide lines is in accord with predictions from a fine-line grain growth model [24].

Results from conventional (double-reservoir) Al(Cu) electromigration test structures [Figure 1(a)] indicate a dependence of the time to failure on grain size [23, 24, 27]. Theoretical models [24, 27, 28] predict that the time to failure for narrow lines should drop as the number of nonbamboo-grained segments increases. The density of nonbamboo-grained segments in a predominantly bamboograined line depends on the median grain size, the spread in the grain size distribution (the wider the distribution, the greater the probability of producing clusters of small grains), and the annealing (grain growth) history of the line. However, experimental results using multilevel Ti/Al(Cu)/ Ti test structures with W studs show that the spread of electromigration failure times is not significantly different among the multigrained, near-bamboo-grained, and bamboo-grained lines, because for such test structures failure occurs by void growth at the cathode end [26].

# Crystallographic texture

Crystallographic texture is a description of the distribution of crystallographic orientations in a population of grains. Texture is usually measured using the X-ray diffraction



TEM micrographs of Al(0.3 wt.% Nb, 0.3 wt.% Pd) lines on an SiO<sub>3</sub>/Si substrate: (a) 0.8  $\mu$ m wide; (b) 2.0  $\mu$ m wide.

pole figure technique. Since thin films are typically fiber-textured (completely symmetric around a fiber axis), the data can be plotted as normalized intensity of an (hkl) plane as a function of tilt angle from the film normal [13]. A film is said to be strongly or tightly textured if most of the intensity lies in a very narrow region located at a specific crystallographic orientation [e.g., (111)], and poorly textured if the main peak is wide or if substantial intensity lies outside the main peak.

The texture in Al and Al-based alloy films usually consists of two components: a crystallographic fiber component [measured as a spread  $\omega$  about a (111) orientation] [29], and a random component (random volume fraction distributed more or less uniformly over all possible orientations). Texture in the films is established during deposition (see **Table 1**) and only slightly strengthened by subsequent annealing, even for annealing temperatures  $\geq 2/3$   $T_m$  [30].

Thin (≈10-25 nm) layers of refractory metals (e.g., Ti, TiN, W) are often employed as adhesion layers or diffusion barriers between the films and the substrate, or as redundant conductors. Such layers can also exhibit strong texture [e.g., (0002) for Ti]. When Al alloy films are deposited onto them, texture inheritance is commonly found [30], producing stronger- or weaker-textured films as a function of the texture strength of the underlying layer.

Four sources of failure have been identified [29] in Al and Al-based alloy films: 1) electromigration, 2) the formation of stress-induced voids, 3) the formation of thermal hillocks, and 4) grain collapse. Film texture has been demonstrated to affect interconnection reliability for single-level metallizations [12, 31–33]. With regard to failure due to electromigration and creep, damage usually occurs heterogeneously at the grain boundaries, indicating that the important aspect of texture is its influence on the distribution of grain-boundary misorientation angles. With

**Table 1** Deposition conditions and associated texture for Al-alloy films deposited in a Varian M2000 single-wafer sputtering system. The Al(0.5 wt.% Cu) target was a ConMag<sup>TM</sup> target with two power settings, one on the inner and one on the outer ring. The Al(1 wt.% Si) target was a VersaMag<sup>TM</sup> target with one power setting. Additionally, an RF bias could be applied during deposition.

ConMag <sup>™</sup> Al(0.5 wt.% Cu) target					
P <sub>Ar</sub> (mtorr)	Power in/out (kW)	T (°C)	Random volume fraction	(°)	
4	4.8/0.6	100	0.1		
4	9.6/1.2	100	0.1	14	
7	9.6/1.2	100	0.1	14	
4	6.0/6.0	100	0.1	13	
4	9.6/0.8	100	0.1	14	

VersaMag™ Al(1 wt.% Si) target

P <sub>Ar</sub> (mtorr)	Power (kW)	T (°C)	Random ω volume (°) fraction
4	6	100	no (111) texture; random grains
7	6	100	0.5
3*	6	100	0.2
20	6	100	no (111) texture; random grains
4	6 + 400 V RF	100	0.25 27
4	6	450	no (111) texture; random grains

<sup>\*</sup>Collimator; this serves as a filter to capture all flux that is not traveling in a path perpendicular from the target to the substrate.

ConMag and VersaMag are trademarks of Varian Associates, Palo Alto, CA.

regard to failure due to hillock growth and grain collapse, plastic deformation within the grains is responsible, implying that the grain orientation within the stress field is the important parameter.

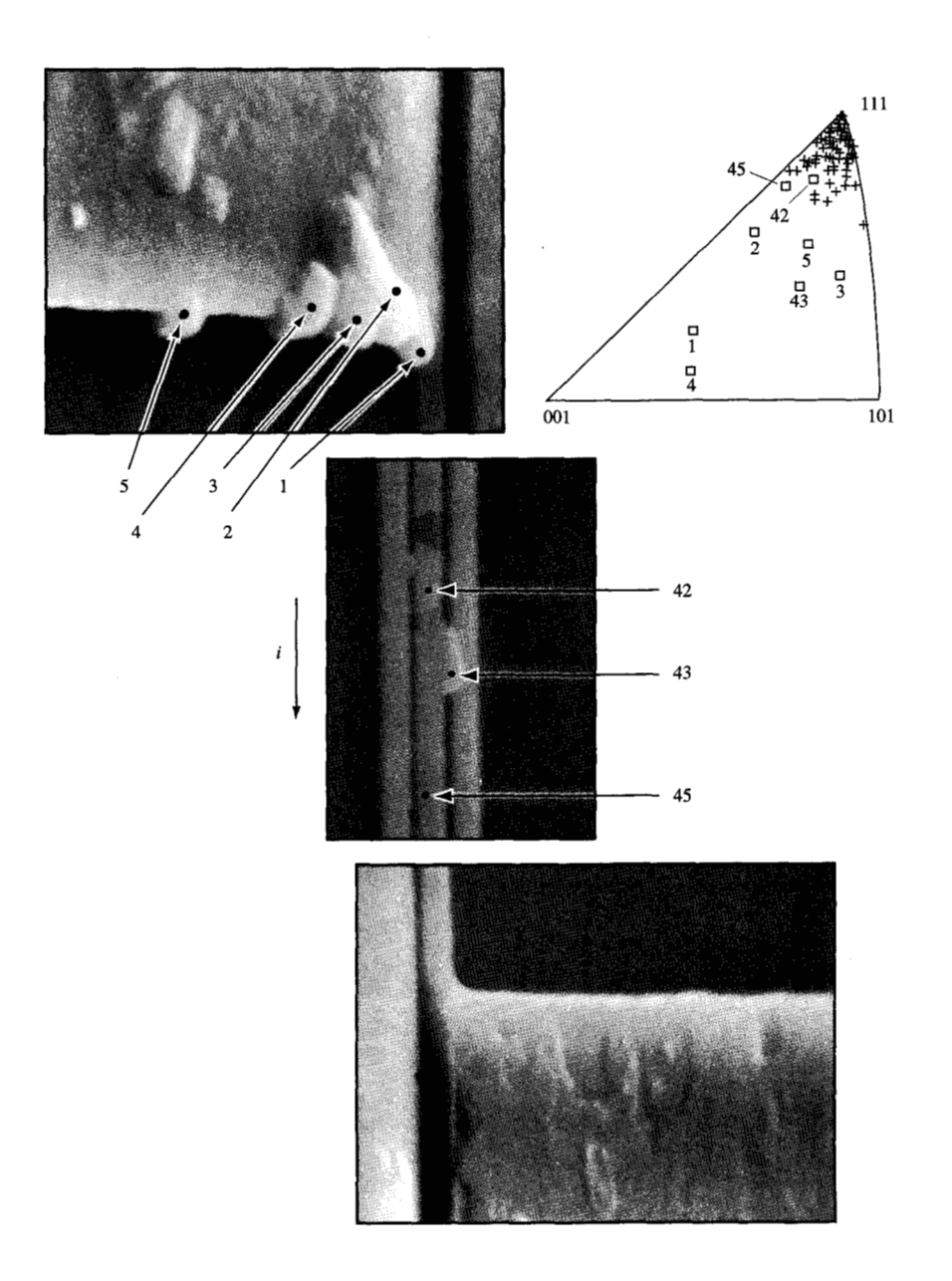
Al and Al-based alloy films usually display a tight (111) texture [most of the grains have (111) planes parallel to the substrate]. Viewed in the direction normal to the film plane, most of the grains differ from each other only by a rotation, which would produce (111) tilt grain boundaries perpendicular to the film plane. For low-angle misorientations (<15°), these boundaries would be composed of a vertical array of parallel edge dislocations. Since in this situation the direction of fastest diffusion (along the dislocation cores) is orthogonal to the film plane, grain-boundary diffusivity is expected to be slower than in a film with poorer texture (e.g., a wider range of misorientations). High-angle misorientations generally produce faster diffusivity paths [except for a limited number of special boundaries known as coincident site lattices (CSL), which behave like low-angle boundaries]. Film texture can also influence mass transport through plastic deformation. Grain orientation (in Al and Al-based alloy films) with respect to the stress field determines the resolved shear stress on the {111} (110) slip systems. Susceptible grains which are deformed display a higher

dislocation density than the remaining population, and should therefore provide greater pipe diffusion. These grains can be sources of flux divergence for electromigration and atomic sinks for stress-induced void growth; they also may act as void nucleation sites.

A scanning electron micrograph (SEM) of a single-level 1- $\mu$ m-thick, 0.45- $\mu$ m-wide Al line which had been damaged by electromigration stressing is shown in **Figure 3**. The corresponding orientations of grains from this sample are plotted on an inverse pole figure. The majority of the grains were strongly (111)-textured, with the exception of the numbered grains, which were generally found to be hillocks or adjacent to damage sites on the line. This is consistent with data on wider lines [34], and shows that grains at which mass accumulates and/or depletes tend to be significantly less textured than surrounding grains. **Figure 4** is a backscattered Kikuchi diffraction (BKD)

inverse pole figure for 25 hillocks from a 1- $\mu$ m-thick Al film (an undamaged  $100 \times 100$ - $\mu$ m<sup>2</sup> Al pad) from a sample comparable to that of Figure 3, which had been annealed at 400°C for one hour. BKD indicates that Al grains which form hillocks collectively exhibit an almost random orientation in comparison to the non-hillock population.

Film deposition conditions can also play a key role in determining texture. Table 1 contains texture results for Al(0.5 wt.% Cu) and Al(1 wt.% Si) films deposited in a Varian M2000 single-wafer sputtering system (onto 125-mm Si/SiO, substrates) under various deposition conditions. The texture of the as-deposited Al(Cu) films was influenced less by the deposition parameters than was the texture of the Al(Si) films. Recent work [34] has shown that the (111) texture strength in Al films increases as the line width decreases, indicating that geometrical confinement by line edges can limit the number and variety of allowed orientations. This has implications for future products, since initial film texture can play a significant role in grain growth, influencing the ultimate grain size and grain size distribution, and controlling the onset of abnormal grain growth [23, 35, 36]. Finer lines containing strongly textured normal grain structures tend to form low-angle grain boundaries with low grain-boundary mobility. However, when abnormal grain orientations are sufficiently different to produce high-mobility, high-angle grain boundaries, abnormal grain growth can occur. Initial texture can also depend upon alloying elements. A 1-µm Al(0.3 wt.% Pd) film was found [33] to have a weak (220) texture, while comparable Al(Cu) and Al(0.3 wt.% Nb, 0.3 wt.% Pd) films displayed strong (111) textures. The addition of 0.3 wt.% Nb to the Al(Pd) film changed its grain size distribution from bimodal to monomodal and changed its texture from (220) to (111). This effect could be explained by the type, location, and distribution of precipitates, which influence film nucleation and in situ grain growth during deposition.



# E COLUMN

SEM micrographs (tilted  $\approx$ 60° from the normal) of a 1- $\mu$ m-thick, 0.45- $\mu$ m-wide Al line after electromigration stressing at  $1 \times 10^6$  A/cm<sup>2</sup> at a temperature of 225°C (anode end is at the top). Also shown is a corresponding backscattered Kikuchi diffraction inverse pole figure for the grains of the line, indicating that most of the grains were strongly (111) textured—with the exception of the numbered grains, which were hillocks or damage sites adjacent to voided regions. (Courtesy J. L. Hurd, IBM Analytical Services, Hopewell Junction, NY.)

# Mass transport

Mass transport constantly occurs in metallic films, especially during annealing, which tends to homogenize the solid solution phases which are present on a macroscopic level through the random walk process of atomic diffusion. Locally, of course, the microstructure varies considerably in composition, orientation, defects, etc., but because this motion is random, there is no net degradation in film

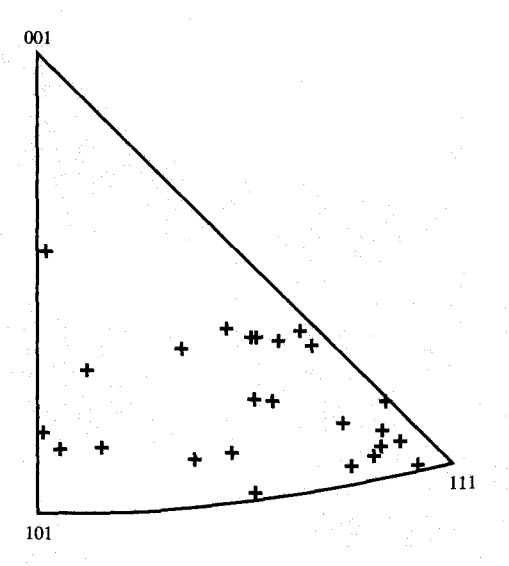


# Figure 4

Backscattered Kikuchi diffraction inverse pole figure for 25 hillocks in a 1- $\mu$ m-thick Al film (from an undamaged  $100 \times 100$ - $\mu$ m<sup>2</sup> region of a pad of a line similar to that of Figure 3) after annealing at 400°C for one hour. The hillocks were more randomly textured than the surrounding grains. (Courtesy J. L. Hurd, IBM Analytical Services, Hopewell Junction, NY.)

properties. Nonrandom (directional) atomic motion can be introduced by application of external forces, such as a thermally induced mechanical stress, an applied voltage, a current, or thermal gradients. Directional atomic motion results in mass transport from one location to another, which may give rise to reliability problems. In this section we describe the theoretical background of mass transport under the external forces of electromigration and mechanically-induced-stress gradients.

An atomic flux along a line segment of an Al or Al-alloy film that is induced by an external driving force  $F_i$  can be characterized by the expression

$$J_{i} = n(D_{\text{eff}}/kT)F_{i}, \qquad (1)$$

where n is the density of atoms able to diffuse with the effective diffusivity  $(D_{\rm eff})$  along the line; T is the absolute temperature of the line segment, and k is the Boltzmann constant.

Several types of diffusional path are possible for the general case of a metal line encapsulated in an insulating material: bulk diffusion, interfacial diffusion, pipe diffusion, grain-boundary diffusion, and surface diffusion. Bulk diffusion, which occurs through the bulk of the line segment, is the slowest. The activation energy for grain-boundary diffusion,  $Q_{\rm gb}$ , is considerably smaller than that for bulk diffusion,  $Q_{\rm g}$  ( $Q_{\rm B} \simeq 1.5-3 \times Q_{\rm ob}$ ), making it

substantially faster; in fact, the presence of a single grain boundary along a metal line having a 1-μm cross section is sufficient to make grain-boundary diffusion dominant! However, grain-boundary structure can vary widely within a given metal line segment, giving rise to considerable variability in diffusivity from boundary to boundary. Grainboundary diffusivities cited in the literature are usually average values measured over a large number of grains having a distribution of orientations, with low-angle boundaries and "special" boundaries yielding the lowest diffusivity values. Although the activation energy for pipe diffusion (diffusion along dislocations) is comparable to that of grain-boundary diffusion, the cross-sectional area of a single dislocation is so small that the net diffusivity clearly depends upon the density of dislocations. Interfacial diffusion (atomic motion along relevant metal/insulator or metal/metal interfaces) is highly dependent on the details of interfaced bonding and structure.

The effective diffusivity  $D_{\rm eff}$  along a fine Al or Al-based alloy line of a given cross section can be characterized as

$$D_{\text{eff}} = D_{\text{B}} + \sum_{j}^{n} D_{\text{gbj}} \left( \frac{\delta_{\text{gbj}}}{d} \right) + D_{\text{I}} \left[ 2\delta_{\text{I}} \left( \frac{1}{w} + \frac{1}{h} \right) \right] + D_{\text{P}} \rho_{\text{disl}} d^{2},$$
(2)

where the subscripts B, gb, I, and P denote bulk, grain-boundary, interface, and pipe parameters, respectively;  $\delta$  denotes grain-boundary or interface width, d is the (average) grain size, w is the line width, h is the line thickness, and  $\rho_{\rm disl}$  is the dislocation density. A free surface diffusion is omitted in Equation (2) because of the assumed presence of a native Al oxide.

Diffusion in narrow Al or Al-alloy lines can be measured by a variation of the marker displacement method (drift velocity technique), using electrical current to generate the applied force. The structure we have used for this measurement is a narrow line deposited over a refractory metal underlayer that is connected to a current supply through an underlying W stud. The marker drift velocity,  $v_{\rm d}$ , is extracted from the derivative of the marker displacement with respect to time. The marker diffusivity (the effective diffusivity) in the line can then be obtained using the Nernst-Einstein relation,  $v_{\rm d}=(D_{\rm eff}/kT)F_{\rm e}$ .

In electromigration, atoms are regarded as being driven in the direction of the "electron wind" [37], causing the cathode end of the line to become depleted. The electromigration driving force  $F_{\rm e}$  can be characterized by the expression

$$F_{\rho} = Z^* e E = Z^* e \rho j, \tag{3}$$

where E is the electric field, e is the magnitude of the charge of an electron,  $Z^*$  is the effective charge number,  $\rho$  is the electrical resistivity, and j is the current density.

Activation energy values reported in the literature for aluminum self-diffusion along a grain boundary, dislocation core, aluminum/aluminum oxide interface, and in bulk aluminum are respectively 0.5 to 0.7 eV [6, 38, 39], 0.8 to 0.9 eV [38, 40], 0.9 to 1 eV [41], and 1.48 eV [42, 43]. The magnitude of the diffusivity decreases progressively in the same order. Typical values of  $D_{\rm eff}$  obtained from marker measurements are plotted in Figure 5. The values for  $D_{\text{eff}} = (\delta/d)D_{\text{gb}}$  were obtained from Reference [39], assuming that  $Z^* = -20$  [6]. The bulk values were calculated by extrapolating the data in Reference [42]. As can be seen, the effective diffusivities in the multigrained and near-bamboo-grained films are clearly much greater than the bulk diffusivity, even at a sample temperature of 315°C ( $\geq$ 194°C = 0.5  $T_{\rm m}$ , where  $T_{\rm m}$  is the melting point of the films). We therefore see that the effective diffusivity in the films is dominated by the fast diffusion paths. This is typical of the behavior of Al and Al-alloy films.

In the case of SV, the driving force arises from a gradient in the chemical potential or the difference in the energy change produced by adding an atom at a void surface or at a dislocation in the highly strained grain interior. A brief review of the causes of stress-induced voiding will clarify how these problems arise. For example, a segment of an Al interconnection line can be represented by a rectangular solid block of Al. At an elevated temperature (e.g., 425°C), this block has equilibrium dimensions  $l_1$ ,  $l_2$ , and  $l_3$ . If the block is left unconstrained and allowed to cool to room temperature, each dimension will shrink by the thermal strain  $\varepsilon_0$  =  $\alpha \Delta T$ , where  $\alpha$  is the thermal expansion coefficient for Al and  $\Delta T$  is the temperature change (i.e., 400°C). However, if the Al block is encapsulated in a rigid box, it will retain its dimensions while it cools, and will experience a thermally generated stress  $\sigma$  in each direction which can be characterized by the expression

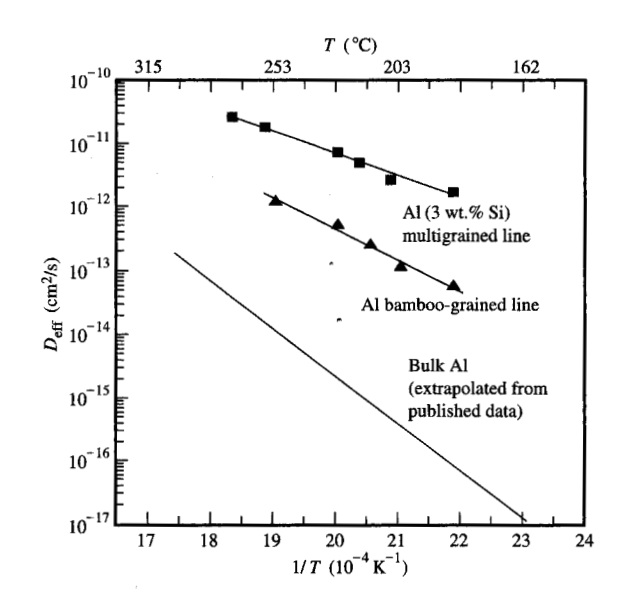
$$\sigma = \frac{E}{(1 - 2\nu)} \, \varepsilon_0 \,, \tag{4}$$

where E is Young's modulus and  $\nu$  is Poisson's ratio. For pure Al,  $\alpha \approx 25$  ppm, producing a thermal strain of about 1% in each direction, or a volume difference about 3% greater than in the unconstrained state.

The constrained Al is highly strained by almost any standard. For example, uniaxial load-deflection curves are used to obtain the yield stress of various metals by identifying the stress at which the sample is deformed inelastically by 0.2%. The strain energy W in an elastically deformed tensile stress sample is given by

$$W = \frac{1}{2} E \varepsilon_0^2 = 4 \times 10^{-6} \frac{E}{2} \,.$$

By comparison, the encapsulated Al sample described above would have a strain energy at room temperature



# Elaure 5

Plots of the effective diffusivity of Al in a 5- $\mu$ m-wide, 0.4- $\mu$ m-thick, multigrained Al(3 wt.% Si) line; a 0.25- $\mu$ m-wide, 0.25- $\mu$ m-thick, bamboo-grained Al line; and bulk Al.

about 100 times that of a conventional tensile test specimen at the tensile yield stress. However, high strain energy by itself would probably not be sufficient to cause voiding if the metal were truly homogeneous. But the existence of crystalline defects such as dislocations and grain boundaries provides sites for vacancy clusters or for the formation of very small cracks, which then become void nucleation sites.

Once a crack has formed, the high strain energy provides the driving force for void growth. Consider the chemical potential, which is the local change in energy caused by the addition or subtraction of an atom. In a homogeneous medium subject to uniform stresses, the chemical potential is the same at all locations. However, the existence of a crack in the strained medium introduces strain relaxation around the crack, a gradient in the strain field, and a corresponding gradient in the chemical potential. The magnitude of the strain energy in an encapsulated interconnection line segment is sufficient to provide a much greater chemical potential in the highly strained grain interior than exists at the surface of a void, causing atoms to migrate from the void to the crystal interior. The chemical potential due to the strain energy can be shown to be given [44] by

$$\mu_{\varepsilon} = \frac{E}{1 - 2\nu} \, \varepsilon_0 \Omega = \sigma \Omega, \tag{5}$$

where  $\Omega$  is the atomic volume of an Al atom; that for an atom at the surface of a void of radius r is given by

$$\mu_{\rm s} \simeq \frac{3\gamma\Omega}{r} \,,$$
 (6)

where  $\gamma$  is the Al surface energy. Equation (6) indicates that the chemical potential of an atom at the surface of a void decreases with increasing void radius. In fact, a minimum radius for such a void can be obtained by equating Equations (5) and (6) and solving for r. Using 1000 ergs/cm<sup>2</sup> as the value for  $\gamma$ , one obtains a void diameter of about 40 Å. This indicates that spontaneous condensation of vacancies into a spherical void is probably not the nucleation mechanism. However, it does show that the strain energy can drive atomic diffusion for very small void sizes, and also indicates that the chemical potential of the void surface can be neglected for voids as small as 0.1 µm in diameter. If voids are assumed to nucleate at microcracks initiated at grain boundaries and these cracks have relatively flat surfaces, the magnitude of the chemical potential may not be an issue at all. The driving force for SV can be written in a form similar to Equation (1) as  $F = \nabla \mu = -\nabla \sigma \Omega$ . However, the meaning is not analogous unless the stress increases linearly over the line length (to produce a constant force), which is generally not the case. Rather, SV is treated more appropriately by the diffusion equation discussed below.

In contrast to electromigration in Al and Al-alloy line segments, which can be continuously accelerated by increasing the temperature and/or the current density, creep voiding has a peak temperature of acceleration which is limited by the deposition temperatures of overlying insulators. This occurs because the two dominant factors (diffusion and stress) which control atomic transport depend on temperature in an opposite manner. Atomic diffusivity increases with increasing temperature, while both the absolute value of mechanical stress and the stress gradient increase with decreasing temperature. At low temperatures, at which the stress in an Al or Al-alloy film on silicon substrate is greatest, diffusivity is small and voids grow slowly. At temperatures at which the insulators are deposited (350-450°C), diffusivity is high, but the stress goes to zero, and both void nucleation and void growth vanish. The temperature for maximum acceleration lies somewhere between these two extremes.

Damage formation in metal lines occurs when there is a net atomic flux, i.e.,  $\nabla \cdot J \neq 0$ , which, in terms of the continuity equation, is expressed as

$$\begin{aligned} -\partial n/\partial t &= \nabla \cdot \mathbf{J} \\ &= \nabla \cdot n(D_{\text{eff}}/kT)F_i , \end{aligned}$$
 (7

where we have used Equation (1) for J. It is evident that any variation in the parameters of Equation (7), such as n,  $D_{\rm eff}$ , T, or  $\sigma$ , along a line segment can cause a flux divergence. The location of such flux divergence sites depends on both the structure of the segment and the test conditions. We emphasize here that it is important to use appropriately representative test structures and experimental conditions to provide useful results which can be used to project relevant interconnection line lifetimes.

# Electromigration

Of the two failure mechanisms discussed in this paper, EM has been studied the longest, and is perhaps the more understood. Traditional EM test lines or "stripes" are fabricated from single-level metallizations, and are useful for understanding factors important to flux divergences. However, circuit chip metallization has become considerably more complex in recent years, involving the use of alloying elements and layered structures with refractory metals such as Ti and W. In addition, chip density has begun to require the use of multiple levels of metallization connected via studs and tapered vias. This has required additional skill in constructing test structures to accentuate structurally induced reliability exposures.

# • Double-reservoir test structures

In a test structure such as that of Figure 1(a), the supply of Al and solute(s) in the narrow region of the line is constantly replenished from the large pad regions [20, 45, 46]. The use of such a test structure can result in overestimating the lifetimes of similar lines in circuit wiring structures, since such lines are usually isolated (rarely contain reservoirs) and therefore may be more vulnerable to failure because of atomic transport away from flux divergence sites—e.g., W vias, silicon contacts, or polysilicon contacts.

• Multilevel test structures without reservoirs

The dominant damage modes observed after accelerated testing of lines using double-reservoir test structures usually reflect the presence of microstructural nonuniformities along the length of the lines [47].

However, if use is made of multilevel test structures without reservoirs [e.g., Ti/Al(Cu)/Ti lines with W studs], damage due to depletion or buildup of material at the ends of the lines may dominate [48, 49]. The presence at the line ends of TiAl<sub>3</sub> and/or W studs or Si junctions prevents Cu and Al from diffusing from one Al(Cu) line segment to another. Solute diffusion, electromigration, and flux divergences at the stud/conductor interfaces must therefore be carefully considered.

In this section, we examine Al line segments connected to W studs or a Ti silicide/Si junction for which local flux

divergences at the contact interfaces are the dominant causes of failure. When subjected to the electromigration force, the diffusion fluxes of Al atoms in the Al line segment J(Al) and through the W studs J(W) are important. The flux difference at an Al-to-W stud interface (assuming no diffusion of Al through the W stud) is

$$J(Al) - J(W) = J(Al) \simeq nv_{d}(Al), \tag{8}$$

where  $v_{\rm d}$  and n are respectively the drift velocity and atomic density of diffusional Al. Material depletion at the cathode end of a conductor line as a result of electromigration causes the resistance of the line to increase. For layered interconnections (Ti /Al(Cu)/Ti, Al(Cu)/W, etc.), the relationship between the rates of material depletion and line resistance change,  $\partial(\Delta L)/\partial t$  and  $\partial(\Delta R)/\partial t$ , can be generally obtained as follows:

$$R(t) = \frac{\rho_{\rm r} \Delta L}{A_{\rm r}} + \frac{\rho_{\rm Al}(L - \Delta L)}{A_{\rm Al}}, \qquad (9a)$$

such that

$$\frac{\partial(\Delta R)}{\partial t} \simeq \left(\frac{\rho_{\rm r}}{A_{\rm r}} - \frac{\rho_{\rm Al}}{A_{\rm al}}\right) \frac{\partial(\Delta L)}{\partial t} \propto \frac{\partial(\Delta L)}{\partial t} = v_{\rm d} , \qquad (9b)$$

where the subscripts r and Al refer to refractory underlayers (e.g., TiN, TiAl<sub>3</sub>, W) and Al-based alloys, respectively;  $\rho$  is the electrical resistivity, A is the cross-sectional area of the specific layer, and L is the initial conductor length. The change in line resistance is simply a linear function of the atomic drift velocity.

Under EM, two opposing transport mechanisms operate in a conductor simultaneously: atomic migration due to the "electron wind" and atomic back-flow due to an electromigration-induced stress gradient. The stress gradient occurs because atoms which are driven out of the cathode end of the conductor accumulate at the anode end, slightly increasing the atomic density with respect to the cathode end. This gradient results in a back-flow of material (Blech effect) [50]. Combining the electron wind and back-flow effects produces a net drift velocity,

$$v_{\rm d} = v_{\rm e} - v_{\rm b} = (D/kT) \left( Z^* e \rho j - \frac{\partial \sigma \Omega}{\partial x} \right),$$
 (10)

where  $v_{\rm e}$  is the electromigration drift velocity and  $v_{\rm b}$  is the average back-flow velocity. An important implication of this effect is that for sufficiently short lines or low current densities, stress can completely suppress mass transport. One can define a threshold value  $\beta_{\rm i}$  [50, 51], for a given  $j_{\rm i}$  and a critical line length  $(L_{\rm c})_{\rm i}$  below which net mass transport vanishes  $(v_{\rm d}=0)$  as

$$\beta_{i} = j_{i}(L_{c})_{i} = \frac{\Delta(\sigma\Omega)_{i}}{Z^{*}e\rho}.$$
(11)

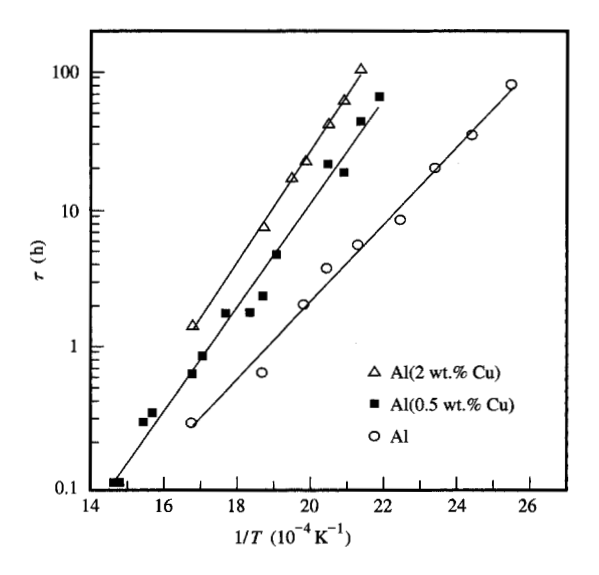


# Figure 6

Mean time to failure for  $2.5-\mu$ m-wide Al(Cu) line/W stud and Al line/W stud two-level test structures at  $10^6$  A/cm<sup>2</sup>, as a function of 1/T. The straight lines are least-squares Arrhenius fits. From [39], reproduced with permission.

The magnitude of EM-induced stress  $\Delta \sigma_i$  is dependent on  $j_i$  for  $\Delta \sigma_i$  less than the fracture strength  $\sigma_c$  of the passivation layer and has a maximum value of  $\sigma_c$ . Hence, for certain applications, careful design can eliminate the risk of EM-related failure.

Different types of Al-alloy films can behave quite differently because the solutes in the films can affect the drift velocity of the solvent atoms differently, depending on the nature of solute-host atom interaction. For example [6], Cu, Cr, and Mg have been found to significantly increase the resistance of Al films to electromigration, while Si [39], Ag, and Au [52] additions do not. Al(Cu) films have been extensively studied since the discovery of the appreciable effect of small additions of Cu on the EMrelated lifetimes of Al films [53]. Al mass transport in Al(Cu) is strongly influenced by the presence of Cu [39, 54]. Figure 6 compares EM-related mean time to failure vs. 1/T for 2.5- $\mu$ m-wide line/W stud test structures fabricated with pure Al, Al(0.5 wt.% Cu), and Al(2 wt.% Cu). As can be seen, the Cu additions substantially enhanced the EM-related lifetime of the test structures, suggesting that the presence of the Cu decreases the Al drift velocity [39]. The electromigration activation energy Q increased from 0.58 eV for pure Al to 0.83 eV for Al(2 wt.% Cu). The value of 0.58 eV, considered

typical for grain-boundary diffusion in Al, has generally indicated [6] that grain-boundary diffusion is responsible for electromigration failure in multigrained Al and Al-alloy lines. The increase in activation energy Q observed for Cu additions can be qualitatively accounted for by a simple trapping model [54]. According to this model, the free vacancy concentration at the grain boundaries is reduced by the presence of Cu due to vacancy-solute binding. This free vacancy concentration decrease reduces the mobility of the Al atoms in the grain boundaries. The problem is complicated by the mechanical back-flow stress which requires that the Cu atoms be swept out a distance comparable to the critical length before the Al will begin to drift [39].

Experiments with multigrained Al(Cu) thin films show that the Cu atoms are initially depleted from the cathode end of a line to a distance approximately equal to the critical length  $L_c$  before observable Al migration occurs [20, 55]. If there is an overhang at the cathode end, this is also depleted and acts as a small reservoir of both Cu and Al. The observed mass transport in the Al(Cu) lines can be separated into three stages: incubation, slow Al motion, and steady state [20, 41]. During the incubation period, Al migration is impeded both by Cu at the grain boundaries and by the presence of the critical concentration of Cu within the critical length, generating a back-flow stress which impedes Al migration.

One can derive relations starting at t=0 for each of these three stages. In the incubation stage, Cu drifts out of the volume contained within the critical length  $L_c$ , prior to the onset of observable Al displacement. The time required before Al displacement begins is designated as the incubation time, which can be defined [assuming  $v_d(\mathrm{Cu}) \propto j$ ] as

$$t_{\rm i} = \frac{L_{\rm c}}{v_{\rm d}({\rm Cu})} = \frac{\beta}{jv_{\rm d}({\rm Cu})} \propto j^{-2}.$$
 (12)

In the second stage, the line length over which the Cu is depleted exceeds  $L_{\rm c}$ , and some Al displacement begins to occur. The Cu depletion zone  $L_{\rm p}$  is defined as the distance from the Al edge at the cathode end of the line to the position where the Cu concentration is high enough to effectively reduce Al diffusion. The drift velocity of Al, e.g., Equation (10), with the added assumption of a mechanical back-flow stress gradient,  $(\partial W_{\rm strain}/\partial x) \propto 1/L_{\rm p}$ , can now be expressed [20] as

$$v_{\rm d}({\rm Al}) = v_{\rm e}({\rm Al})(1 - L_{\rm c}/L_{\rm p}).$$
 (13)

Within  $L_{\rm p}$ , a back-flow stress is generated owing to the motion of the Al atoms by the EM driving force, which retards their migration.

An expression for the time dependence of the Al edge displacement  $\Delta L(t)$  [assuming  $v_{\rm d}({\rm Cu}) = V_{\rm Cu} = {\rm constant}]$ ,

can be derived from Equation (13). At the end of the incubation time  $t_i$ ,

$$L_{p} = L_{c} + v_{Cu}t - \int_{0}^{t} v_{d}(t) dt'$$

$$= v_{Cu}(t + t_{i}) - \int_{0}^{t} v_{d} dt'$$

$$\simeq v_{Cu} \left[ (t + t_{i}) - \left\{ \frac{1}{v_{Cu}} \int_{0}^{t} v_{d} dt \rightarrow 0 \right\} \right]$$

$$= v_{Cu}(t + t_{i}), \qquad (14)$$

where  $t_{\rm i}v_{\rm Cu}=L_{\rm c}$ , and the integral over  $v_{\rm d}$  is eliminated because of the much larger value of Cu drift velocity compared to that of Al. Substituting this expression for  $L_{\rm p}$  into Equation (13) and integrating over time gives

$$\int v_{\rm d} dt = v_{\rm e}(Al) \int_0^{t'} dt - \frac{L_{\rm c}}{v_{\rm Cu}} \int_0^{t'} \frac{1}{t + t_{\rm i}} dt,$$

$$\Delta L = v_{\rm e}(Al) \left[ t - t_{\rm i} \ln \left( 1 + \frac{t}{t_{\rm i}} \right) \right]. \tag{15}$$

To calculate the transient time of the slow-motion stage  $t_s$  under the assumption  $t_s \ll t_i$ , Equation (15) becomes

$$\Delta L = v_{e}(Al)(t_{s}^{2}/t_{i})/2$$
, or  $t_{s}^{2} = 2[\Delta L/v_{e}(Al)]t_{i}$ ,

which results in

$$t_{\rm s} \propto j^{-1.5}.\tag{16}$$

After a considerable amount of time, the length of  $L_{\rm p}$  increases until  $L_{\rm p} \gg L_{\rm c}$  and a steady-state period  $t_{\rm ss}$  and associated constant velocity  $v_{\rm d}$  are attained. The additional edge displacement  $\Delta L_{\rm ss}$  in this period should be a linear function of j, namely

$$t_{ss} = \Delta L_{ss} / v_{s}(Al) \propto j^{-1}. \tag{17}$$

The mean time to failure,  $\tau$ , is assumed to be the time necessary to grow a void to the size needed to produce the resistance shift specified by failure criteria. In general terms,  $\tau \approx t_{\rm i} + t_{\rm s} + t_{\rm ss}$ , assuming that all of the indicated stages of damage occur. Equations (12), (16), and (17) are all consistent with the usual assumption that  $\tau$  is related to the current density  $j^m$ , with m having a value from -2 to -1. The predicted value for m is in good agreement with a reported experimental value of  $m = -1.7 \pm 0.2$  for two-level Ti/Al(2 wt.% Cu)/Ti line-W stud interconnections [39].

For short Al(Cu) lines, the drift velocity of Cu is affected by both the back-flow (just as Al is affected) and the Cu concentration gradient. The Cu mass flow equation [39] becomes

$$-\partial n_{C_0}/\partial t = \nabla \cdot J,\tag{18a}$$

$$J = n_{Cu} v_{d}(Cu), \tag{18b}$$

$$v_{a}(Cu) = v_{a}(Cu) - [D_{ch}(Cu)/n_{Cu}] \partial n_{Cu}/\partial x - \partial (\sigma \Omega_{a})/\partial x,$$
 (18c)

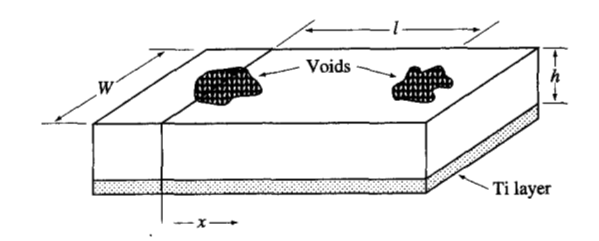
where  $v_{\rm d}({\rm Cu})$  is the drift velocity of Cu in Al(Cu),  $v_{\rm e}({\rm Cu})$  is the drift velocity of Cu solute atoms under the electromigration driving force,  $D_{\rm ch}({\rm Cu})$  is the chemical diffusivity of Cu, and  $n_{\rm Cu}$  is the Cu concentration along the line at a distance x measured from the cathode end. However, as a practical matter, exact solutions to Equations (13) and (18) are not possible because the stress gradient and the chemical diffusivities of Al and Cu are unknown.

# Stress-induced voiding model

Diffusion is generally accepted to be the mass transport mechanism by which mechanical stress-induced voiding (void growth) occurs. In contrast to the case of electromigration, which occurs in the presence of a constant electrical force  $Z^*eE$ , void growth occurs in response to a gradient in the strain field (which can also be expressed as gradients in the stress field or in atomic density). Thus, while it is possible to describe the atomic flux during void growth by J = nuF, as for electromigration, where u is the mobility, both n and Fvary in both space and time, making this approach analytically inconvenient. A more suitable approach is to apply Fick's Law for diffusion, J = -Ddn/dx, although it is conceptually difficult to deal with the "diffusion" of stress or strain. However, diffusing atoms can lead to changes in the local atomic density, which can be related to the local strain as follows: Let  $N_{\rm A}$  be the equilibrium atomic density in atoms/cm3 at the temperature of interest. An applied triaxial tensile strain  $\varepsilon_{10} = \varepsilon_{10} + \varepsilon_{20} + \varepsilon_{30}$ (where 1, 2, 3 refer to the principal axes) produces a reduced atomic density  $n(\varepsilon_{10}) = N_A/(1 + \varepsilon_{10})$ . At some point in time, the strain is relaxed by the diffusion of additional atoms into the strain volume, which produces a position-dependent strain field,  $\varepsilon_{\cdot}(x)$ . An intermediate position-dependent atomic density,  $n[\varepsilon(x)] = N_A/[1 + \varepsilon_1(x)]$ , can be calculated which depends upon and corresponds to the strain field. The difference  $\eta$  between the initial reduced density and the intermediate density is the density (or concentration) in atoms/cm<sup>3</sup> of new atoms responsible for relaxing the strain:

$$\begin{split} \eta(x) &= n[\varepsilon(x)] - n(\varepsilon_0) = \frac{N_A}{1 + \varepsilon_t} - \frac{N_A}{1 + \varepsilon_0} \\ &= \frac{N_A(\varepsilon_{t0} - \varepsilon_t)}{(1 + \varepsilon_{t0})(1 + \varepsilon_t)} \,. \end{split}$$

Differentiating  $\eta(x)$  with respect to position produces



Segment of a metallic line containing a Ti underlayer and encapsulated with an insulator. The line is assumed to contain two voids separated by distance l.

$$\frac{d\eta(x)}{dx} = -\frac{N_{\rm A}}{1+\varepsilon_{\rm 10}}\frac{d\varepsilon_{\rm t}}{dx}\left[\frac{1}{1+\varepsilon_{\rm t}} + \frac{\varepsilon_{\rm 10}-\varepsilon_{\rm t}}{\left(1+\varepsilon_{\rm t}\right)^2}\right] \simeq -N_{\rm A}\frac{d\varepsilon_{\rm t}}{dx}$$

for small values of  $\varepsilon_{\rm t}$  and  $\varepsilon_{\rm t0}$ . Since  $\varepsilon_{\rm t0} \leq 0.03$  at room temperature, this approximation is adequate for most purposes, and we see that the gradient in the concentration of new atoms is proportional to the negative gradient in the triaxial strain; i.e., the strain decreases as the concentration of new atoms increases. Since stress is propositional to strain, this implies that the stress is relaxed by the diffusion of new atoms. The driving force for diffusion is the gradient in atomic density which is produced by the stress, and not due to stress as an additional independent factor.

The difficulty in predicting void growth in a metal line resides primarily in knowing in advance the nucleation site density and magnitude of strain in the line. The former requires a knowledge of the dependence of nucleation sites on the microstructure of the line, while the latter requires knowledge of the thermal and mechanical properties of the encapsulating materials, which are not always available. However, isothermal void growth can be analytically modeled, and can be compared with void sizes observed over time. Our approach [56] applies the one-dimensional diffusion equation

$$\frac{\partial \eta}{\partial t} = -D \frac{\partial^2 \eta}{\partial x^2} \tag{19}$$

to the situation depicted in **Figure 7**, where two voids are separated by a distance l in an Al line segment of thickness h and width w, having a Ti underlayer and encapsulated in an insulator. For this treatment, the insulator encapsulating the line is assumed to be perfectly rigid, preventing the Al from relaxing. D is the metal self-diffusivity, and  $\eta$  is the concentration of atoms diffusing into the volume between

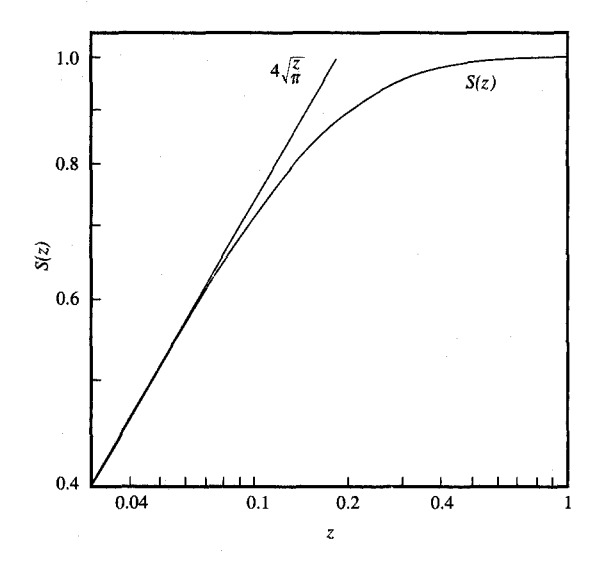


# Figure 8

Predicted void growth function S(z), where  $z = Dt/l^2$ .

0 and l to relieve stress. The boundary conditions and initial condition for the solution are

$$\eta(x, 0) = 0 \text{ for } 0 < x < l$$

and

$$\eta(0, t) = \eta(l, t) = N_0, \tag{20}$$

where  $N_0 = (\Delta V/V)N_{\rm A} = 3\varepsilon_0N_{\rm A} = 3\alpha\Delta TN_{\rm A}$ .  $N_{\rm A}$  is the atomic density in Al,  $\alpha$  is the thermal expansion mismatch between the Al and surrounding insulation,  $\Delta T$  is the temperature difference between passivation deposition and aging temperatures, and  $\varepsilon_{\rm t}$  has been replaced by  $3\varepsilon_0$  (rigid box approximation) for simplicity. The solution to Equation (19) with the conditions specified in Equation (20) is found by separation of variables to be

$$\eta(x, t) = -\frac{4N_0}{\pi} \sum_{m_{\text{odd}}}^{\infty} \frac{1}{m} \sin\left(\frac{m\pi x}{l}\right) e^{-(m\pi/l)^2 D t},$$
 (21)

which is a series of sine functions on x modified by exponentials in time. The atomic flux out of one side of the void can then be calculated from Fick's Law:

$$J(0, t)|_{T=\text{const}} = D \left. \frac{\partial \eta}{\partial x} \right|_{x=0}$$

$$= \frac{4N_0 D}{l} \sum_{m=0}^{\infty} e^{-(m\pi/l)^2 D t}.$$
(22)

The volume contributed by this flux is then given by

$$V(t)_{+} = \Omega A \int_{0}^{t} J(t') dt', A = wh,$$

$$= \frac{4N_{0}\Omega Dwh}{\pi} \sum_{m_{b+1}}^{\infty} \int_{0}^{t} e^{-(m\pi/l)^{2}Dt'} dt'.$$
(23)

The + subscript indicates that the volume calculated is due to flux to the right (positive x) only. Simplifying the expression via a change of variables,  $z = Dt/l^2$ , and performing the integration, we obtain

$$V(t)_{+} = V_{f+}(8/\pi^{2}) \sum_{m_{\text{odd}}}^{\infty} \frac{1 - e^{-m^{2}\pi^{2}z}}{m^{2}}$$

$$= V_{f+}S(z), \tag{24a}$$

where  $V_{f^+}=3\varepsilon_0whl/2$  is the maximum void volume that can be formed from the material on one side of the void. Void separation is likely to be distributed randomly such that the calculation of individual void volumes requires knowledge of these specific spacings. However, assuming an average spacing  $\overline{l}$  over a large population of voids, the average void volume can be given by

$$\overline{V(t)} = V_{\bar{f}} S(z), \tag{24b}$$

where  $V_{\bar{f}} = 3\varepsilon_0 wh\bar{l}$ . S(z) is shown in **Figure 8**. For small z, corresponding to short times, small diffusivities (low temperature), and large separations between voids,  $S(z) = 4\sqrt{z/\pi}$ . In this regime, the stress midway between the voids is generally not relaxed. For large z, corresponding to long times, large diffusivities (high temperature), and small separations between the voids, S(z) approaches 1, corresponding to the complete relaxation of all stress between the voids. Thus, for times before void growth saturation, we can write  $V(t) = C_0 t^{1/2}$ .

# Results and discussion

# • Electromigration

# Double-reservoir test structures

The first Si integrated circuit interconnections were fabricated from pure Al films. Si was added to the Al films to prevent shorts due to Al penetration into the Si junctions (spiking). Cu was added to extend electromigration lifetime [53], and more recently has been shown to extend stress voiding lifetime as well [57, 58]. Al(Cu) and Al(Si, Cu) alloys are both widely used in industry today. In Al(Cu) alloys, the electromigration resistance is enhanced as the Cu content increases from 0 to ~4 wt.% Cu [52]. Various other solute additions (e.g., Pd + (Nb, Si, Cu, V) [59–61], Sc [62, 63], and

Cr, Ag, Au, Mg [6, 64]) have shown promising properties and are the subject of much current research. The use of a Ti underlayer was introduced to reduce contact resistance and to serve as a diffusion barrier [65]. Films consisting of layers of Al alloys and refractory metal layers such as Ti, TiN, TiW, and W also provide an effective reduction in hillock formation and enhanced electromigration performance [66–70]. The incorporation of the refractory layers also helps to prevent the formation of resistive ternary compounds, improves the texture of the Al-alloy layers, and suppresses both electromigration and stress-induced void formation.

Thermal processing (cycling) steps encountered during integrated circuit chip fabrication are critical in establishing the microstructure of the circuit wiring, especially if the wiring consists of binary and more complex alloys in which second-phase precipitation and/or layer reaction occurs. Figure 9 [71] depicts the range of process temperatures during the fabrication of one level of a typical circuit wiring structure containing a sputterdeposited Al(0.5 wt.% Cu) film 0.3 to 2  $\mu$ m thick. During deposition, substrate temperature is controlled from room temperature to 550°C, depending on the amount of conformality needed. After deposition, the film is patterned by photolithography and reactive ion etching (RIE) and annealed at 400°C. Next, a conformal insulating layer (such as SiO<sub>2</sub>) is deposited and patterned by photolithography and RIE, and interlevel connections are formed by means of chemical-vapor-deposited (CVD) W studs. These steps are repeated in order to complete the desired multilevel structure. Subsequent packaging and chip attachment temperatures can also exceed 300°C. The Al(Cu) films are thereby subjected to a complex series of thermal treatments during processing which results in Al grain growth and Al<sub>2</sub>Cu ( $\theta$ -phase) formation, dissolution, and precipitation. With Al(0.5 wt.% Cu), all of the Cu is dissolved into solution above 310°C [72]. Therefore, annealing at temperatures greater than 310°C causes dissolution of the  $\theta$  precipitates. The cooling rate from the single-phase region determines how much Cu is quenched into solid solution in the Al grains. Annealing at temperatures below 310°C results in 1) the precipitation of Cu-rich precipitates from the Cu that is quenched into the Al grains, and 2) a coarsening of the Al, Cu precipitates [14, 73, 74].

In patterned Al(2 wt.% Cu) lines, θ-phase precipitation is strongly dependent on the line width, with more precipitates found in finer lines (**Figure 10**). The Cu concentration at room temperature in Al grains in both blanket films and patterned lines after quenching (-200°C/minute) from annealing temperatures <350°C was equal to the Cu solubility in Al [14]. After annealing at higher temperatures, the Cu concentration in the grains of fine lines was substantially lower than the solubility at the

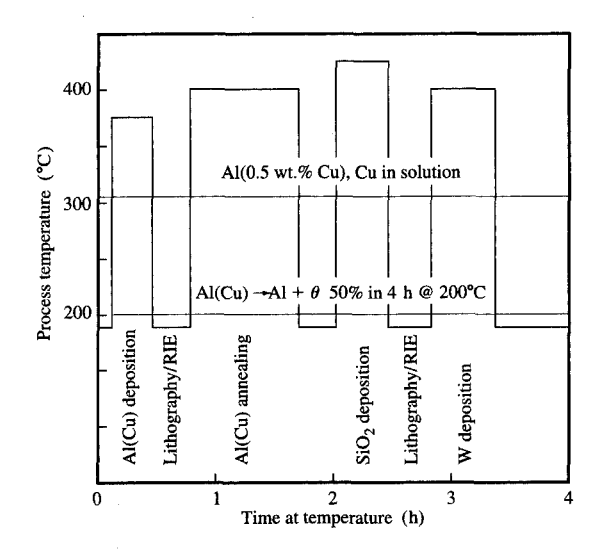


# Figure 9

Temperature cycles encountered during the fabrication of a typical  $Al(Cu)/SiO_2/W$  stud interconnection structure. This sequence is repeated (2–5 times) to form the lines of IBM multilevel, on-chip interconnections. From [71], reproduced with permission.

annealing temperature (approximately 1/3 that at 500°C). The lower density of fast diffusion paths (i.e., grain boundaries) in narrow lines, compared to that of blanket films and/or wider lines, should increase the time required for Cu to dissolve into the fine-line Al grains, since it is controlled by bulk diffusion. The  $\theta$  precipitate blocking sites (precipitates which completely traverse the line) per 50  $\mu$ m of line length were counted as a function of line width for the Al(2 wt.% Cu) sample shown in the figure. The blocking sites were found to number 14 for the 0.5- $\mu$ m-wide line, 8 for the 1.1- $\mu$ m-wide line, and <2 for the 1.8-µm-wide line. Therefore, the number of blocking boundaries appears to increase as the line width decreases [14]. The significance of this result on single-level (double-reservoir) line reliability is shown below. A 3× improvement in the electromigration  $t_{50}$  lifetime (at 200°C,  $1 \times 10^6$  A/cm<sup>2</sup>) was observed for 0.5- $\mu$ m-wide, single-level Al(0.5 wt.% Cu) samples which had been rapidly cooled from 400°C (quenched) compared to those which had seen an additional low-temperature annealing at 250°C for 144 hours (quenched/aged) [14]. However, 1-μm-wide lines were unaffected by such annealing. The difference in the electromigration behavior of the 0.5-μm-wide lines was found to be due to the different film microstructures formed in the patterned lines as a function of annealing history. The quenched samples contained fewer flux

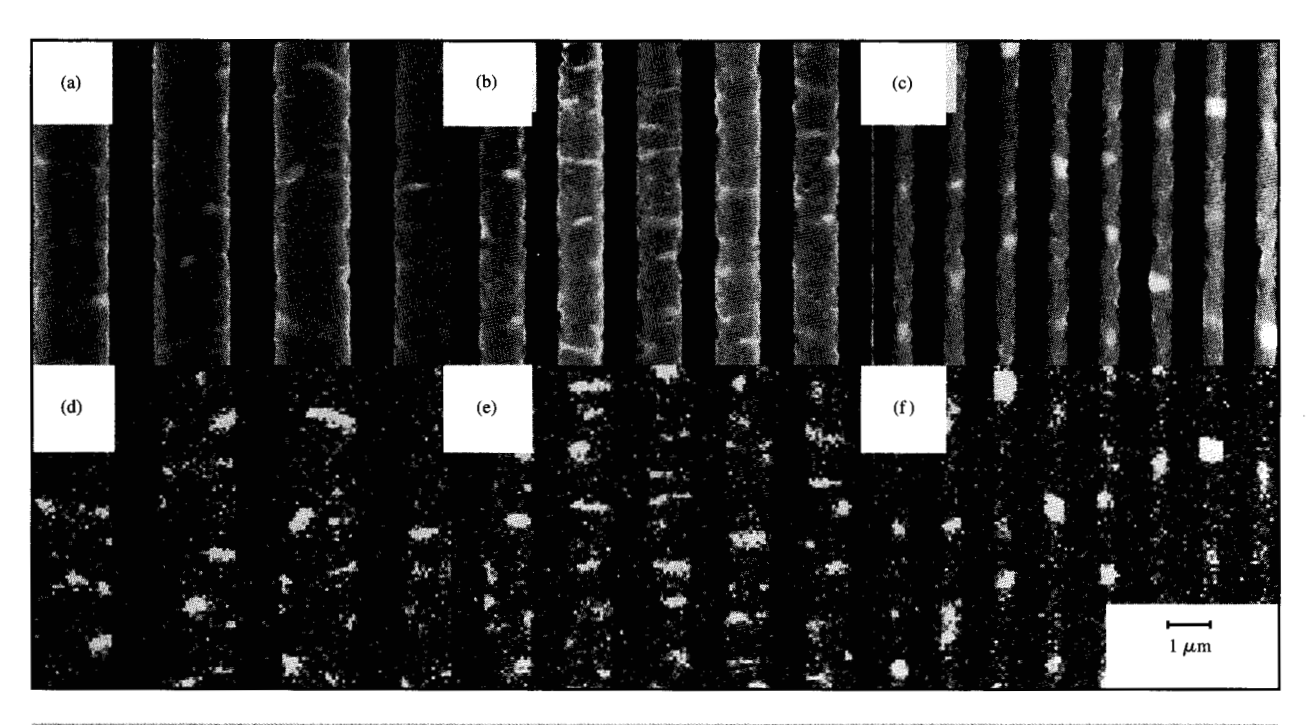


# Figure 10

Secondary-electron images [(a), (b), and (c)] and Cu  $K_{\alpha}$  X-ray digital images [(d), (e), and (f)] of 1- $\mu$ m-thick Al(2 wt.% Cu) patterned lines: 1.8  $\mu$ m wide [(a) and (d)], 1.1  $\mu$ m wide [(b) and (e)], and 0.5  $\mu$ m wide [(c) and (f)]. The sample containing the lines was preannealed at 500°C for one hour, rapidly cooled to room temperature, and subsequently aged at 300°C for four hours. From [14], reproduced with permission.



# Ballicak

TEM micrograph of a blocking  $Al_2Cu$  precipitate in an 0.6- $\mu$ m-wide A1(0.5 wt.% Cu) line which had been annealed at  $400^{\circ}C$  for one hour, quenched to room temperature at a rate of  $200^{\circ}C$ /min, and aged at  $250^{\circ}C$  for 144 hours. From [71], reproduced with permission.

divergence sites [i.e.,  $\theta$ -phase precipitates which formed completely across the width of the patterned line (**Figure 11**)] than the quenched/aged samples. In contrast, the wider  $(1-\mu m)$  lines displayed similar microstructures in both their quenched and quenched/aged conditions. Thus, for single-level Al(Cu) lines, microstructure and EM-related reliability appear to be linked.

# Transport mechanisms

The dominant damage sites in double-reservoir accelerated test structures occur at points of flux divergence, which vary according to the microstructure and morphology along the sample under test. For multilevel structures [e.g., Al(Cu) lines on W studs or in contact with Si junctions], the flux divergences exist at the contact interfaces. Our previous investigation [39] of the Al(Cu)-W junction have indicated that failure occurs differently than in double-reservoir test structures; namely, the Al<sub>2</sub>Cu precipitates of the Al(Cu) were found to dissolve sequentially from the cathode end. When a critical length of Al was cleared of precipitates, Al started to migrate from the cathode. With time a void was created at the cathode end. Thus, failure was dominated by the mass depletion at the cathode, which is unlike conventional double-reservoir tests in which the flux divergences occur mostly at grain-boundary junctions along the line. In this section, we describe the use of a test structure without reservoirs to examine diffusion in multigrained and bamboo-grained Al-alloy lines under the influence of the EM driving force.

Three possible rapid diffusion paths in a multigrained Al-alloy line tested in air are depicted in **Figure 12**:

1) along the central grain boundary; 2) along the line edges and line faces; and 3) along freshly formed surfaces [75]. Diffusion along the line edges is attributed to the combination of atoms diffusing through the grain boundaries connected to the line edges and along the interfaces. The curvatures of the trailing surfaces have sharp maxima at their tips, indicating that surface energy can also contribute to the driving force. After testing in air, two fine trails of residue were left, which were assumed to be Al oxide. Lines passivated with 100-nm-thick Si<sub>3</sub>N<sub>2</sub> displayed a faster migration rate and did not form a trail of residue, presumably because the Al was not exposed to oxygen.

Figure 13 [76] shows a sequence of SEM micrographs of the cathode end of a 0.85-µm-wide bamboo-grained Al(Pd, Nb) line having a W underlayer after electromigration testing at  $0.8 \times 10^6$  A/cm<sup>2</sup> at a temperature of 300°C for 7, 16, and 33 hours, respectively. As can be seen, the line narrowed from the cathode (left) end and widened at the anode end (not shown); this could be attributed to interfacial and surface diffusion. As the testing continued, the first grain boundary began to open and widen despite the fact that it was normal to the direction of electron flow, with no network of connected grain boundaries. Migration in the first grain ceased because the length of the remaining segment was less than the critical length. Disappearance of single-crystal grains and narrowing of the bamboo-grained regions in the line could be explained by interfacial mass transport. However, the mass transport rate along the edges of bamboo-grained lines is slower than along the edges of multigrained lines, suggesting that interfacial diffusion in the lines is slower than grain-boundary diffusion, since two fast paths (grain boundary and interfaces) are connected to the line edges in the multigrained structure. Al atoms which move away from the grain boundary connected to the line edge at the cathode are expected to generate excess vacancies which should be able to migrate along the interface. This should result in a mass transport rate, along the line edges in the multigrained lines, which is similar to the edge displacement rate due to grain-boundary diffusion (see Figure 12). Among the differences we found between Al(Cu) and Al(Pd, Nb) lines was the difficulty in observing the narrowed line effect in Al(Cu) bamboo-grained lines. This suggests that diffusion in the trailing "pure Al" portion of Al(Cu) bamboo-grained lines is relatively rapid and that the associated depletion front (trailing surface) can easily catch up with the Al line edge (interface) diffusion. Interestingly, studies of electromigration in bicrystal Al lines, some via [77] in situ TEM [78, 79], have also indicated that both interfacial and grain-boundary diffusion contribute to the resulting damage.

Evidence of Cu diffusion from Al(Cu) lines along the Al/native Al oxide or Al/TiAl<sub>3</sub> interfaces can be inferred

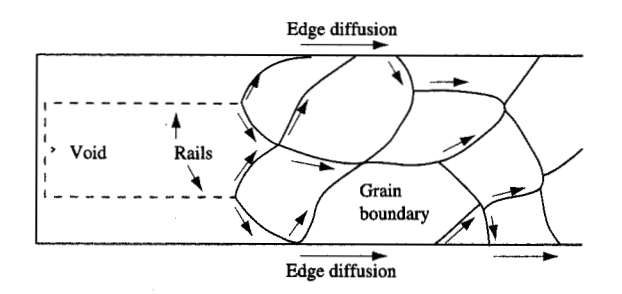


# Figure 12 Possible rapid diffusion paths in a multigrained Al-alloy line.

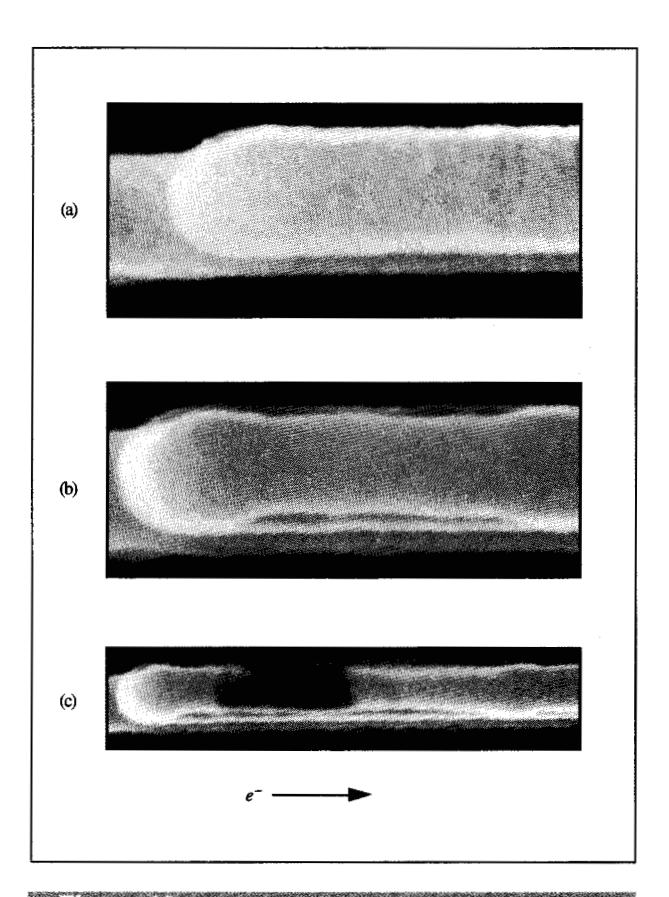
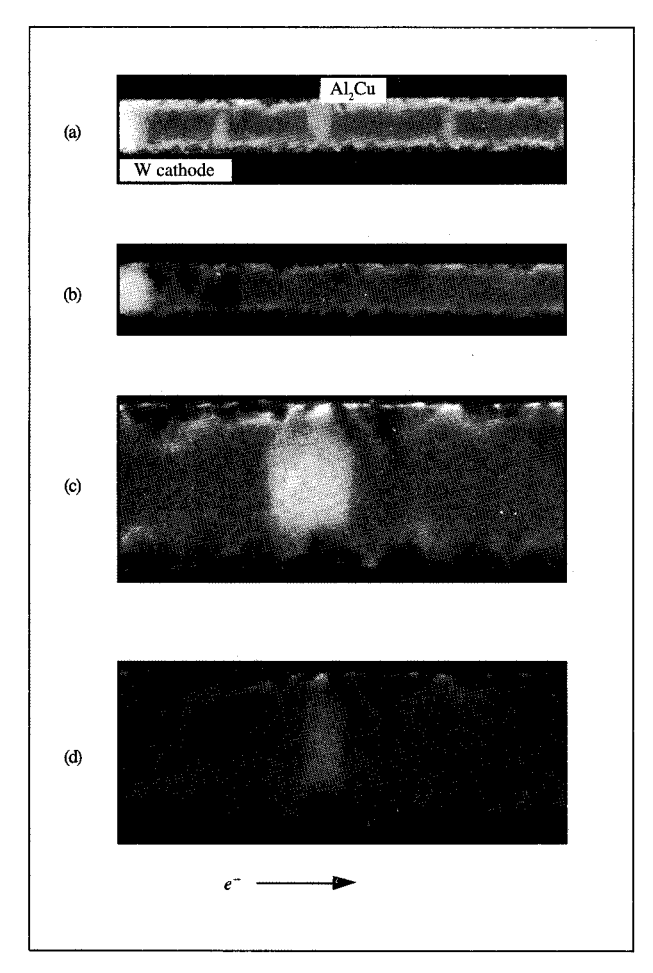


Figure 13

SEM micrographs of the cathode end of an Al(Nb, Pd) bamboograined line having a W underlayer, after testing at  $0.8 \times 10^6$  A/cm² at a temperature of 300°C (a) for 6 hours, (b) for 16 hours, and (c) for 33 hours.

from the electromigration results from a 0.7- $\mu$ m-wide, bamboo-grained Ti/Al(4 wt.% Cu)/ Ti line with W studs,



SEM micrographs of  $0.7-\mu$ m-wide Ti/Al(4 wt.% Cu)/Ti lines after testing at  $0.8 \times 10^6$  A/cm<sup>2</sup> at a temperature of 250°C (a) before testing, (b) after testing for 61 hours, (c) 22 hours, and (d) 43 hours. The micrographs indicate that the Al<sub>2</sub>Cu precipitate in (c) and (d) is the same precipitate as the largest one in (a). From [76], reproduced with permission.

as depicted in **Figure 14** [76]. The bright spots on the micrographs are Al<sub>2</sub>Cu precipitates. The largest precipitate shown in Figure 14(a) is also shown in Figures 14(c) and 14(d) with a  $3 \times$  magnification. A Cu depletion zone of 3  $\mu$ m from the W cathode stud was observed after 22 hours of testing. Continued testing resulted in the complete disappearance of precipitates from a 7- $\mu$ m length, as shown in Figure 14(b), which indicates that the Cu solute drifted a distance of 7  $\mu$ m in 61 hours. The possibility of Cu diffusion through the lower and upper TiAl<sub>3</sub> layers was considered to be unlikely because of its extremely low diffusivity in TiAl<sub>3</sub> at 250°C, 2 × 10<sup>-17</sup> cm<sup>2</sup>/s [80]. Furthermore, it was determined that there was no grain-boundary network throughout the bamboo-grained line. A

high-precision measurement of substitutional Cu diffusivity in Al has been reported [81] with use of a radioactive tracer-sectioning technique. Using this value for the bulk diffusivity of Cu in Al [81], the value of the Cu effective charge number,  $Z^*$ , would have to be  $\approx -1400$  in order to explain the observed behavior. This is substantially higher than the published values of  $Z^* = -7$  in bulk Al [82] and  $Z^* = -4$  to -15 in Al thin films [83]. Thus, it appears that the previously proposed interfacial diffusion mechanism in Al(Pd, Nb) bamboo-grained lines can be equally applied to Cu in Al(Cu) films. Initially, the Cu solute concentration is in equilibrium with the Cu in the grains, interfaces, grain boundaries, and Al<sub>2</sub>Cu  $\theta$  precipitates. In the presence of a current, the Cu is depleted from the cathode end along various interfaces. When the concentration is reduced below the solubility limit locally, e.g., at interfaces, whatever Cu may be present at the boundaries and/or in the grains is a source of supply of Cu for the interfaces. Thus, the Cu is removed from the Al and, ultimately, the Al<sub>2</sub>Cu  $\theta$  precipitates dissolve to maintain the equilibrium solid solubility level. As expected, the first Al<sub>2</sub>Cu precipitate to dissolve is that nearest to the cathode end. When Figures 14(c) and 14(d) are compared, the precipitate can be seen to have dissolved primarily from the cathode side as well (although this is not always the

Multigrained film results: Comparisons with predictions Accelerated test structures containing 1.9-µm-wide, multigrained Ti/Al(2 wt.% Cu)/Ti/TiN lines having a W underlayer and passivated with SiO, were used to examine the validity of the proposed model. The test structures contained two 300- $\mu$ m-long lines which were linked by W studs and two short, underlying Ti/Al(2 wt.% Cu)/ Ti/TiN lines. The length of the underlying lines was 8 μm, which was chosen to be less than the critical length in order to ensure that mass depletion occurred only in the overlying lines. A 200-nm-thick W underlayer was used in order to reduce the amount of joule self-heating, which occurs when voids form in the overlying lines. As the voids grow at the cathode end during an electromigration experiment, all of the current passes through the more resistive W underlayer, which serves as a bridge between the studs and the remaining overlying lines. Typical plots of resistance change vs. time and current density at 255°C are shown in Figure 15. The resistance change  $[\Delta R = R(t) - R_0]$  after the initial incubation period was a consequence of Al mass depletion away from the Al(Cu)/W stud interfaces, where  $R_0$  is the initial line resistance prior to current flow. Note that the incubation time,  $t_0$ , defined in resistivity measurements is not the same as the  $t_1$ defined in the edge displacement experiments. The incubation time in resistance measurements is measured at the time when the resistance starts to increase. In an edge

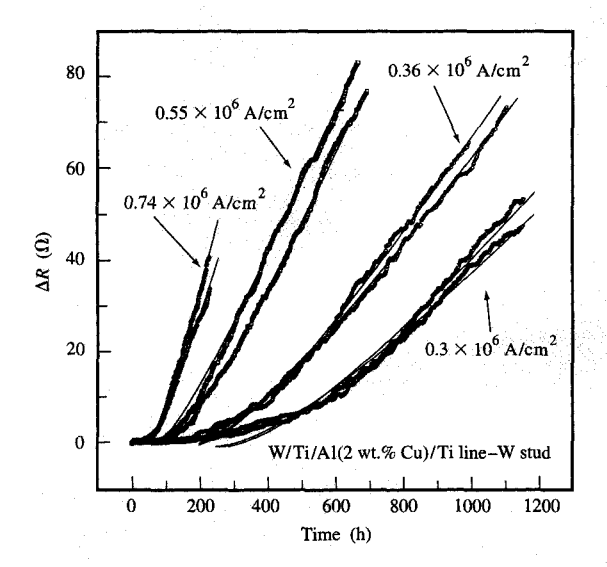
displacement experiment, it corresponds to the time taken for the Al to separate from the Al(Cu)/W stud interface ( $\Delta L_0 = 2~\mu \text{m}$ ). Use of the simple ratio  $L_0/t_0$  to calculate the drift velocity would be in error because it ignores the different stages of the damage process. One may write a relation between the edge displacement  $\Delta L$  and line resistance change  $\Delta R$  for the 1.9- $\mu$ m-wide line as

$$\Delta R = (\Delta L - \Delta L_0)[\rho(W)/A(W) - \rho(Al)/A(Al)]. \tag{25}$$

The edge displacement ( $\Delta L$ ) is given by Equation (15). The curves shown in Figure 15 are the result of fitting the data to Equation (25) using two adjustable parameters,  $t_i$  and the steady-state  $\partial(\Delta R)/\partial t$ . The qualitative fit of the data by this simple model is relatively good. The values of  $t_i$  and  $\partial(\Delta R)/\partial t$  are extracted from the least-squares fitting of these data. The relation between  $t_i$  and  $j^m$  gives a value of  $m = -1.7 \pm 0.2$ . A linear relation between the steadystate  $\partial (\Delta R)/\partial t$  was observed for j up to  $1 \times 10^6$  A/cm<sup>2</sup>. These values are consistent with the predicted values from Equations (12) and (17). For current densities  $>1.5 \times 10^6$ A/cm<sup>2</sup>,  $\Delta R(t)$  (not shown) cannot be fitted by this model because of excessive joule heating from the W bridging underlayer. The rate of resistance change at  $j > 1.5 \times 10^6$ A/cm<sup>2</sup> for 0.75- $\mu$ m-thick Al(2 wt.% Cu) lines continually increased with time, reflecting the effect of joule heating.

# Critical length effect

The above EM-related failure mechanisms, related to the presence of abrupt material junctions, are also applicable to lines which are in contact with Si junction areas [84, 85]. These are most susceptible to electromigration damage under the dc pulsed currents typically used in CMOS circuitry. Typically, Figures 16(a), (b) show changes in the resistance of 0.7-\u03c4m-wide Ti/TiN/Al(2 wt.\u03c8 Cu, 3 wt.\u03c8 Si) lines as a function of time and line length at 250°C. The lines were in contact with TiSi<sub>2</sub>/polysilicon through a Ti/TiN barrier layer. The Al(Cu, Si) lines were 0.6  $\mu$ m thick and 0.7  $\mu$ m wide, passivated with SiO<sub>2</sub>, and the contact vias were 1.2  $\mu$ m in diameter and 0.3  $\mu$ m in height. Electromigration damage was found to be negligible in the 25- $\mu$ m-long lines subjected to  $j = 1.2 \times 10^6 \text{ A/cm}^2$ [as indicated in Figure 16(a)] and in both the 25- $\mu$ m and 50- $\mu$ m-long lines for  $j = 0.5 \times 10^6$  A/cm<sup>2</sup> [as indicated in Figure 16(b)], reflecting the short-length effect predicted by Equation (10). Figure 16(c) shows the line resistance change as a function of time for several 30- $\mu$ m-long Al(Cu) lines having W stud contacts after being subjected to a current density of  $2.0 \times 10^6$  A/cm<sup>2</sup> at a temperature of 250°C. The time-dependent line-resistance-change curves of the short lines are all similar. It should be noted that if the experimental value of the critical length for EM-induced stress is less than the fracture strength of the SiO<sub>2</sub>, the critical length depends on geometry, SiO<sub>2</sub> passivation layer preparation, etc.

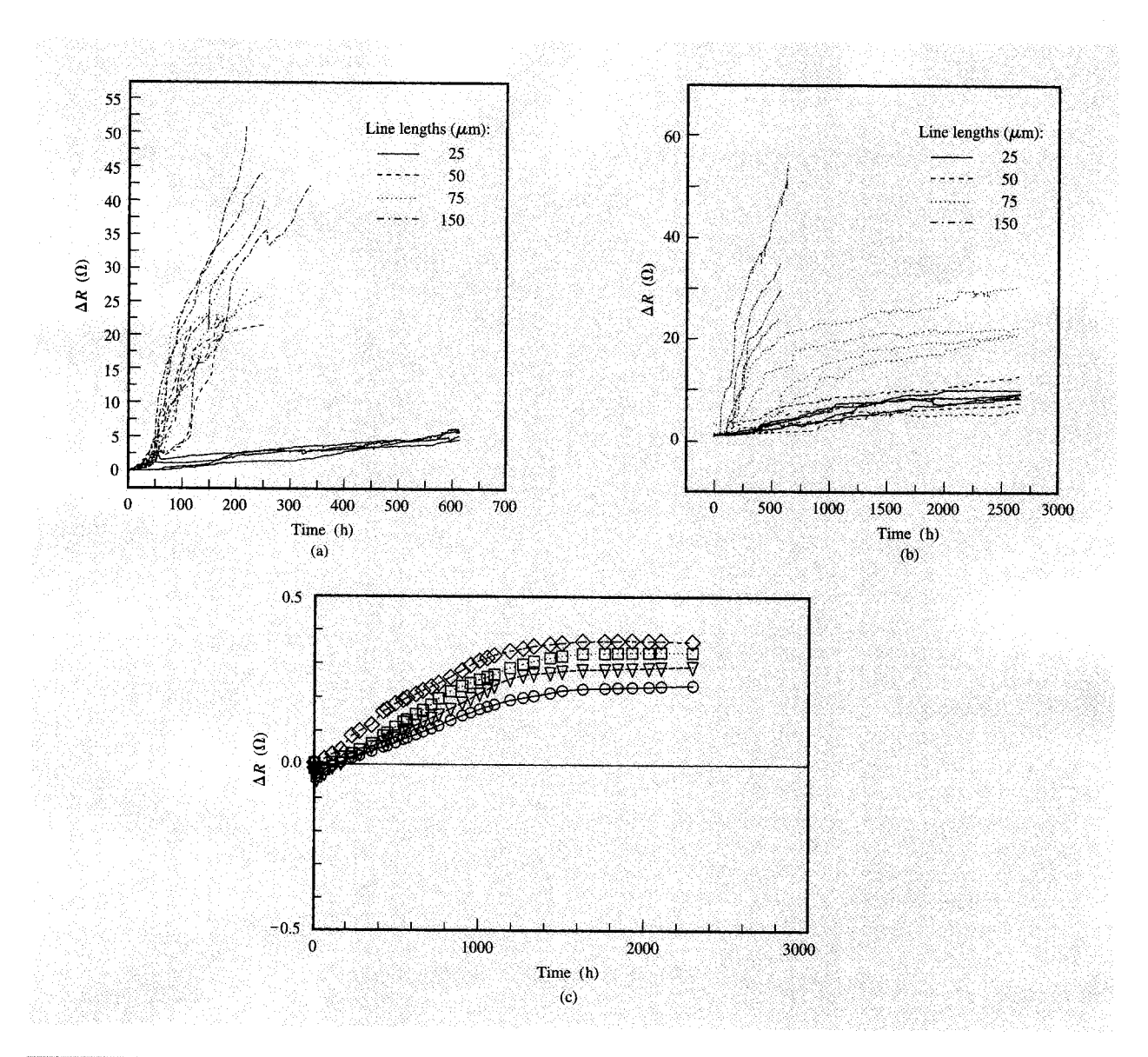


# Flaure 15

Change in resistance of 1.9- $\mu$ m-wide test-structure lines as a function of time, at 255°C and different current densities ( $R_0 \approx 25~\Omega$ ). Curves are least-squares fits. From [76], reproduced with permission.

The above-mentioned short-length effects associated with isolated lines can obscure EM and SV phenomena if care is not given to the selection of the test structure. For example, because contact and via chain structures are commonly used for resistance characterization purposes, it is tempting to use them for EM and SV studies. However, the short-length effect in via chains could easily lead to the overlooking of potentially catastrophic failures from void formation in long lines connected to these via chains.

Multigrained and bamboo-grained test structures Typical resistance changes,  $\Delta R(t)$ , as a function of time and current density for SiO<sub>2</sub>-passivated bamboo-grained Ti/Al(0.5 wt.% Cu)/Ti/TiN-W stud samples at 260°C are shown in Figure 17. The resistivity of the Al(0.5 wt.% Cu) is 3.05  $\mu\Omega$ -cm at 25°C. The overlying SiO, thickness is approximately 0.4  $\mu$ m. As a result of interfacial and grain-boundary diffusion, broken line segments were also observed. When coupled with the large joule heating from its underlying TiAl, layer, the time-dependent resistance curves differ from those of Equation (25). In order to eliminate this complication from data interpretation, the electromigration mean-time-to-failure  $\tau$  is defined here as the time necessary for a 2% resistance increase; this is estimated to be equivalent to about a 0.5-\mu movement of Al away from the W stud. For the associated, short



Parts (a) and (b): Change in resistance of 0.7- $\mu$ m-wide Al(2 wt.% Cu, 3 wt.% Si) lines as a function of time, at current densities of 1.2  $\times$  10<sup>6</sup> A/cm<sup>2</sup>, and 0.5  $\times$  10<sup>6</sup> A/cm<sup>2</sup>, respectively; (c) change in resistance of short (30  $\mu$ m in length) Al(0.5 wt.% Cu) lines as a function of time. The lines of (a) and (b) were terminated at Si contacts; those of (c) were terminated at W stud contacts. Part (c) from [45], reproduced with permission.

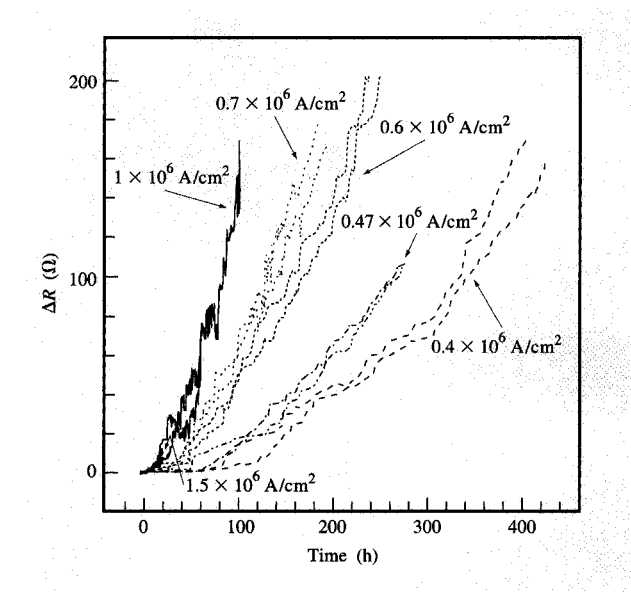
section of TiAl<sub>3</sub>, the joule heating effect is not significant for  $j \le 1.5 \times 10^6$  A/cm<sup>2</sup>. **Figure 18** shows a plot of  $\tau$  as a function of current density, using the 2% criterion. By using a standard expression,  $\tau = \tau_0 j^m$ , the value of m was found to be  $-1.7 \pm 0.3$ , which is consistent with the proposed simple model.

Values of  $\tau$  as a function of 1/T for several types of lines are plotted in **Figure 19**. [Data for pure Al lines are also plotted (see the section below for details).] In the test

structures used, the size of the underlying W studs scales with the width of the test lines; hence, finer lines require a smaller total displacement to migrate beyond their smaller W cathode studs. The resulting equivalent mean lifetimes for the narrow lines (0.7  $\mu$ m wide) and wide lines (1.9  $\mu$ m wide) are therefore an artifact of test structure design. The edge displacement rate of the Al(Cu) bamboo-grained lines was actually 2–3× slower than that of the multigrained lines. Note that in this case the drift velocity effect was

limited to the initial slow-motion regime [see Equation (13)]. An electromigration activation energy O of  $0.87 \pm 0.04$  eV was obtained for both the 1.9- $\mu$ m and 0.7-µm-wide lines. Only four diffusion paths are possible in the narrow bamboo lines; bulk diffusion, pipe diffusion (down dislocations), interfacial diffusion at the edges of lines (along the native aluminum oxide/aluminum interface), and Al/TiAl, interfacial diffusion. Bulk diffusion is several orders of magnitude slower than grain-boundary diffusion, and significant pipe diffusion requires a dislocation density of the order of  $10^3/\mu m^2$  to produce results consistent with those that are typically observed. TEM observations of fine lines show dislocation densities below  $2/\mu m^2$  (T. Shaw, IBM Thomas J. Watson Research Center, Yorktown Heights, NY, November 1994, private communication), ruling out pipe diffusion. Hence, it appears that diffusion along the edges of lines is about 1/3 that in grain boundaries for Al(Cu) lines in the initial slow Al(Cu) motion period. Graphic evidence of sidewall interfacial diffusion is provided by the morphology of the displaced edges of a void formed in a bamboo-grained line as a result of mass depletion at the cathode end (Figure 20, after SiO, passivation layer removal). Interestingly, the above activation energy is in good agreement with the reported values of  $0.86 \pm 0.05$  eV, the electromigration activation energy for Cu in Al(Cu, Si) thin films [39] and 0.87 to 1.0 eV, the grain-boundary activation energy of Cu diffusion in Al films [6]. This activation energy is maintained even at sample temperatures above the solubility limit, indicating that distributed Cu atoms, not Al, Cu precipitates, are responsible for limiting the Al movement (although the availability of Cu atoms is directly linked to the number and size of the precipitates).

Typical cumulative % failure data (defined at 2%, corresponding to  $\approx 0.5 \mu m$  of Al having been depleted from the W stud) for passivated Al(Cu) lines are plotted in Figure 21. The lifetime distribution can be fitted by either a normal or a log-normal distribution. Typical  $\sigma$  [6] values for log-normal failure distributions for 1.9- $\mu$ m and 0.7- $\mu$ mwide lines are about 0.2. The small uncertainty in the distributions is primarily due to well-defined void growth at the cathode end, and partly due both to the domination of the diffusion process by Cu and to the presence of fast diffusion paths along the Al/oxide or Al/TiAl, interfaces. The effect is especially apparent in isolated narrow lines, which show less variation than double-reservoir lines. In the latter case, failure is strongly dependent on local variations in microstructure, which produces a broader distribution of failure times. Thus, when the mass transport for electromigration is controlled by Cu diffusion, reservoir effects are eliminated by material discontinuities. sidewall diffusion is present, and the local variation in microstructure plays a less crucial role in determining the distribution width.



# Element 17

Typical changes in resistance of  $SiO_2$ -passivated, 0.7- $\mu$ m-wide, bamboo-grained Ti/Al(0.5 wt.% Cu)/Ti/TiN-line-W stud samples as a function of time, at 260°C and different current densities. From [76], reproduced with permission.

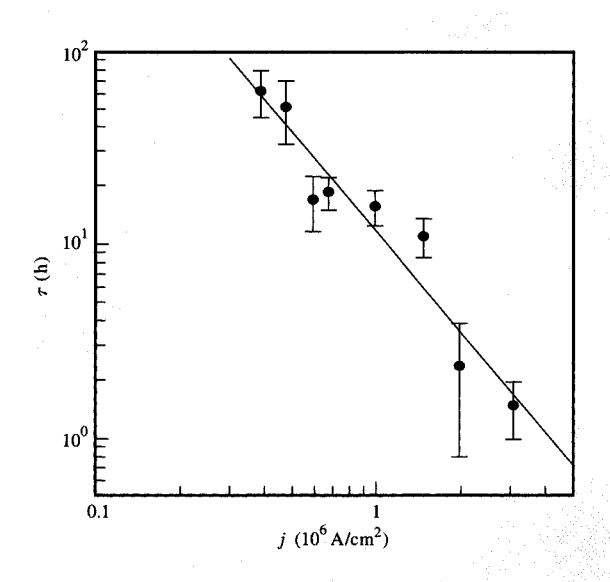
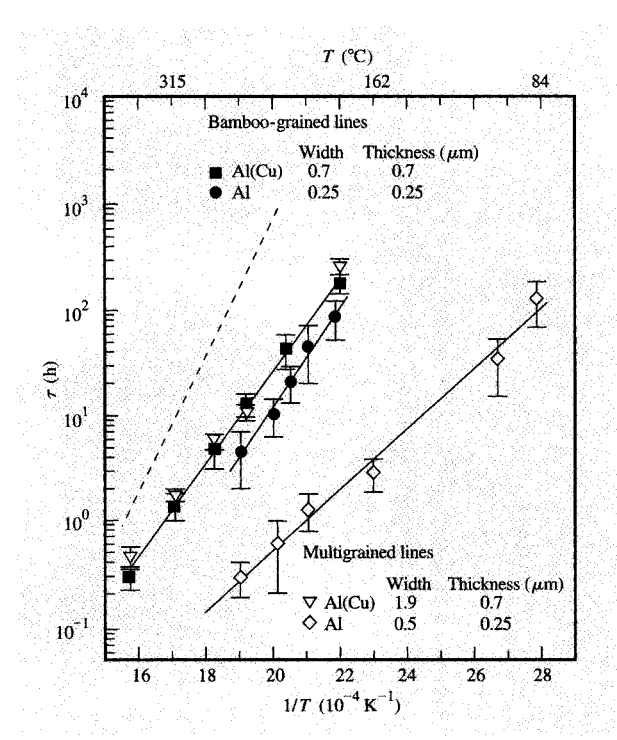


# Figure 1

Plot of  $\tau$  vs. j on logarithmic coordinates, for samples similar to those of Figure 17. The straight line is a least-squares fit to the data.



# Entitlede

Plot of  $\tau$  vs. 1/T for several types of Al(Cu) lines. The solid lines are least-squares fits; the dotted line is estimated using bulk diffusivity from [42], and assuming that  $Z^* = -20$ .

# Electromigration in 0.25-µm-wide lines

A study of electromigration in single-level overlapped Al/W unpassivated lines 0.25  $\mu$ m wide was carried out in order to investigate EM-related failure in Al films at that line width. An underlayer Ti(10 nm)/W(30 nm) was defined by reactive ion etching. The Al lines were deposited via an e-gun and patterned by a lift-off process using electronbeam lithography. The Ti/W underlayer and the 0.5-μm and 0.25- $\mu$ m-wide by 0.25- $\mu$ m-thick pure Al lines were overlapped at both ends of the Al line by 0.6  $\mu$ m. The Al line length was 200  $\mu$ m. Prior to the tests, all of the samples were annealed at 400°C in He for three hours. The resistivity of Al was found to be 4  $\mu\Omega$ -cm with a temperature coefficient of resistivity =  $2.9 \times 10^{-3}$ /°C. This resistivity is substantially higher than the usual value of 2.65  $\mu\Omega$ -cm for pure Al, indicating that impurities were probably incorporated into the Al.

Figure 22 shows an SEM micrograph of the cathode end of the 0.25- $\mu$ m-wide Al line having wider, underlying W contacts, after testing for six hours at 225°C at  $j = 1 \times 10^6$  A/cm<sup>2</sup>. A region of Al depletion nearly 0.5  $\mu$ m long at the cathode end is shown. The electromigration lifetime, obtained from open current failures, which

corresponded to approximately 0.6 µm of Al depletion at the cathode end, was that plotted in Figure 19 as a function of 1/T. An electromigration activation energy of  $0.96 \pm 0.1$  eV was obtained, compared to the activation energy of 0.58 eV for a 0.5- $\mu$ m-wide multigrained Al line. For comparison, data for the 1.9- $\mu$ m and 0.7- $\mu$ m-wide, 0.8μm-thick multigrained and bamboo-grained Ti/Al(0.5 wt.% Cu)/ Ti lines and the estimated time for the depletion of 0.6 µm of Al from the cathode end, using Al bulk diffusion data [42, 86] and  $Z^* = -20$  (at  $j = 1 \times 10^6$  A/cm<sup>2</sup>), were also plotted in Figure 19. The similar electromigration activation energies in the former two cases (as indicated by their similar slopes) suggests that mass transport along the Al/oxide interfaces may also be the dominant mechanism in the near-bamboo-grained Al lines, as it appears to be for the Al(0.5 wt.% Cu) lines. Although a detailed TEM examination of the dislocation content of these lines has yet to be done, the dominant mass transport mechanism in the bamboo-grained lines appeared to be interfacial diffusion, whether or not Cu was present.

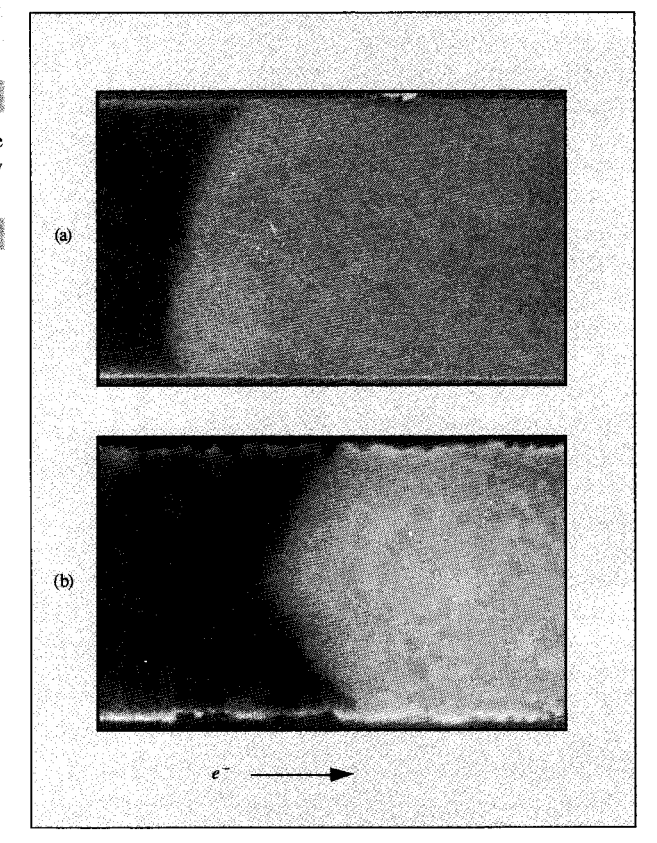


# Figure 41

SEM micrographs (after removal of SiO<sub>2</sub> passivation) of electromigration damage in (a) Al(Cu) multigrained line and (b) Al(Cu) bamboo-grained line.

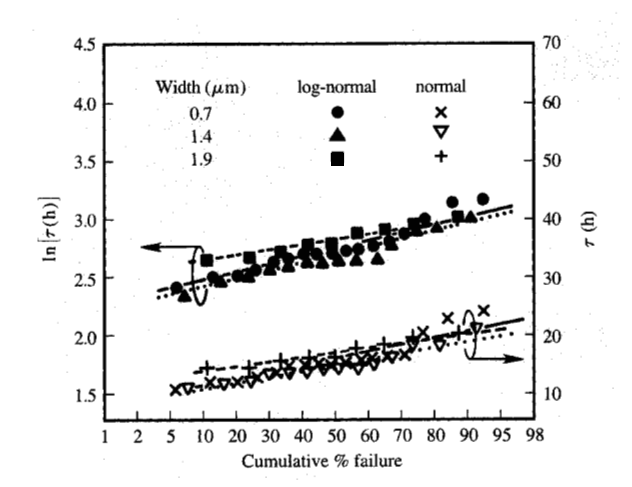
# Stress-induced voiding

Stress-induced voiding (SV) most generally occurs in narrow ( $<4-\mu m$ -wide) Al lines. The problem was first documented in 1984 [87] and has been extensively studied and reviewed [88]. It arises from high levels of tensile hydrostatic stress produced by the encapsulating dielectrics, which are relatively rigid (e.g., SiO<sub>2</sub> or Si<sub>3</sub>N<sub>4</sub>), as discussed earlier. Small notches usually nucleate at high-stress locations (such as line edges and topological steps) and grow with time until the Al becomes discontinuous. For interconnections fabricated from a single layer of Al-alloy film, this results in open circuit failure. For layered (redundant) metallizations (using, for example, W, TiW, or Ti), discontinuity causes an increase in line resistance, which can affect circuit timing and performance, and accelerate electromigration failure. Void growth is accelerated by increasing the testing temperature or increasing the stress in the Al-alloy film (e.g., by depositing the insulating layer at higher temperatures).

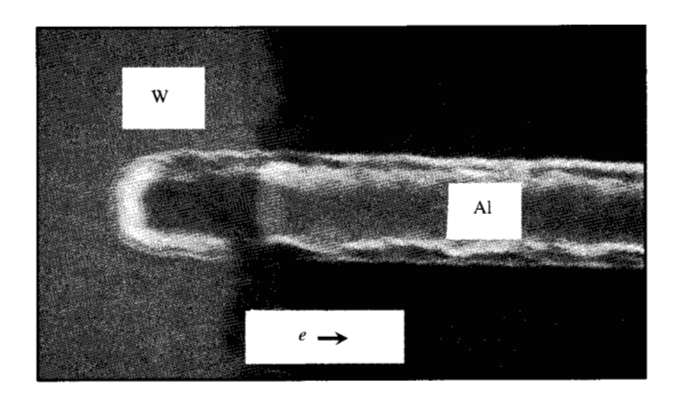
As a failure mechanism, SV has more than its share of undesirable characteristics. First, failure by SV has not always been readily predictable, as it seems to be for EM-related failure. This is because SV failure in nonlayered Al-alloy metallizations depends upon void size, shape, and density, as well as upon the specific alloy used and its microstructure and processing. Second, accelerated testing is not as effective as for EM because the physical processes involved are not generally as well understood, and because an upper limit to the acceleration is imposed by the nature of the forces governing atom transport. Furthermore, lines cannot be forced to fail by SV if they have insufficient mechanical stress, or if the alloy microstructure inhibits void nucleation and/or growth. Indeed, failure by SV can be dependent on wafer location, and can vary from wafer to wafer. Finally, the nucleation of voids and initial growth rates are strongly influenced by local geometry, which is not a circuit design issue, but rather a process control issue. Because relatively small changes in structure can produce substantial changes in stress in the Al-alloy films, and because metallization microstructure can have large local variations, controlling void nucleation can be difficult. Some of these diffusivities are evident in the following discussions.

# Voiding in layered test structures

As in EM, the presence of a refractory, redundant layer under and/or over an Al(Cu) layer can reduce the possibility of open circuit failure by SV with the layer. Voiding damage then produces only resistance shifts and increases susceptibility to EM-related damage. However, with multilevel interconnections, locations at line/stud interfaces may still exist which are vulnerable to open circuit failure by voiding. The possible existence of such



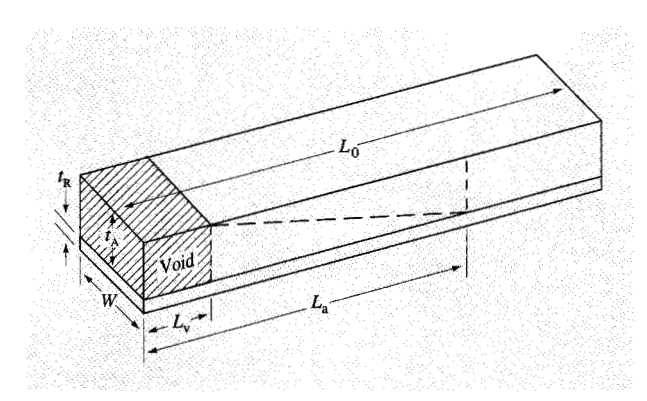
Typical cumulative % failure data for passivated Al(Cu) lines, plotted on both normal and log-normal scales. From [76], reproduced with permission.



SEM micrograph, showing edge depletion at the cathode end of a  $0.25\text{-}\mu\text{m}$ -wide Al line having wider, underlying W contacts.

locations necessitates expanding our understanding of voiding mechanisms.

Fortuitously, the presence of the refractory, redundant layer provides an electrical means for measuring void growth. In the absence of a redundant layer, void measurement must be accomplished by optical or scanning electron microscopy. With the redundant layer present, the resistance increase in an Al-alloy line caused by the presence of a void which makes it discontinuous is directly proportional to the size of the void through the resistance of the remaining redundant strip. Consider a line of length  $L_0$ , width w, and thickness  $t_A$ , which has a redundant



# Flaure 23

Simplified representation of a void in a metallic line of length  $L_0$ , having a redundant underlayer of thickness  $t_{\rm R}$ . The increase of the resistance of the line due to the presence of the void is approximately proportional to the ratio of void length to line length, as indicated by Equation (26). The length of the void is related to the atomic self-diffusion length  $L_{\rm a}$  through Equation (27).

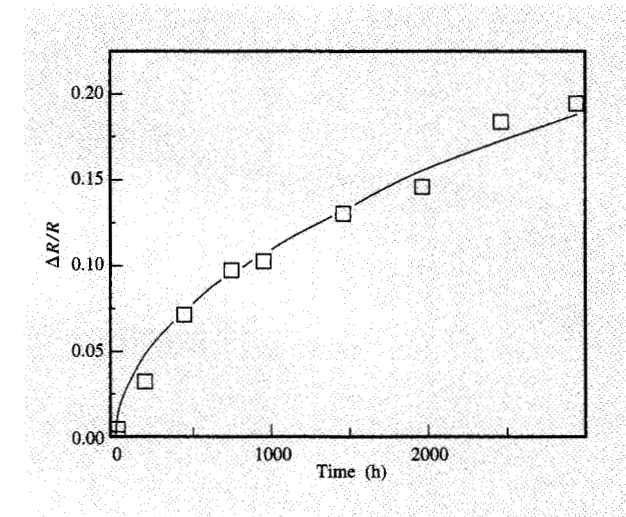


# Figure 24

Least-squares fit of fractional resistance change vs. time during the aging at 225°C of a 0.4-\(\mu\)m-wide, 0.35-\(\mu\)m-thick, 800-\(\mu\)m-long Al(0.5 wt.% Cu, 1 wt.% Si) line having a redundant underlayer.

layer of thickness  $t_{\rm R}$ , as shown in Figure 23. For the case in which a single void of length  $L_{\rm v}$  is present in the line, the resistance of the line is given by

$$R = \frac{\rho_{\rm R} L_{\rm v}}{A_{\rm R}} + \frac{\rho_{\rm A} (L_0 - L_{\rm v})}{A_{\rm A}} = \frac{L_{\rm v}}{w} \left[ \frac{\rho_{\rm R}}{t_{\rm p}} - \frac{\rho_{\rm A}}{t_{\rm A}} \right] + \frac{\rho_{\rm A} L_0}{t_{\rm a} w} \,,$$

where  $\rho$  is the resistivity and the subscripts R and A denote redundant metal and Al-alloy, respectively; the last term is the unvoided line resistance,  $R_0$ . The fractional resistance shift is then given by

$$\frac{\Delta R}{R_0} = \frac{R - R_0}{R_0} = \frac{L_v}{L_0} \left\{ \frac{\rho_R t_A}{\rho_A t_R} - 1 \right\} \simeq \frac{L_v}{L_0} \frac{\rho_R t_A}{\rho_A t_R}, \tag{26}$$

because the factor in resistivity and thickness is generally >1.

Time dependence can be introduced into Equation (25) through the time dependence of  $L_{\rm v}$ . As already shown, void volume exhibits a square root dependence on time before the stress reservoir is depleted. Replacing S(z) with  $4\sqrt{Dt/l^2\pi}$  in Equation (24b), we obtain

$$\frac{V(t)}{wh} = \frac{V(t)}{wh}$$

$$= \frac{3\varepsilon_0 whl}{wh} \frac{4}{l\sqrt{\pi}} \sqrt{Dt}$$

$$= \frac{12}{\sqrt{\pi}} \varepsilon_0 \sqrt{Dt} = \frac{1}{\sqrt{\pi}} \frac{\Delta V}{V} (2L_a),$$
(27)

where  $L_{\rm a}$  is the atomic self-diffusion length. Equation (27) indicates that the void volume is proportional to the atomic diffusion length on both sides of the void times about half the excess volume created by strain. Substituting Equation (27) for  $L_{\rm v}$  into Equation (26), we obtain

$$\frac{\Delta R}{R_0} = \frac{\rho_R t_A}{\rho_A t_R} \frac{12\varepsilon_0}{L_0 \sqrt{\pi}} \sqrt{Dt}.$$
 (28a)

For the general case, a line of arbitrary length can be expected to contain more than one void, with each void contributing to the resistance increase. A factor of  $N_{\rm v}$ , the number of voids in the line being tested, must therefore be included in the equation, resulting in

$$\frac{\Delta R}{R_0} = \frac{\rho_R t_A}{\rho_A t_R} \frac{12\varepsilon_0}{L_0 \sqrt{\pi}} N_v \sqrt{Dt}.$$
 (28b)

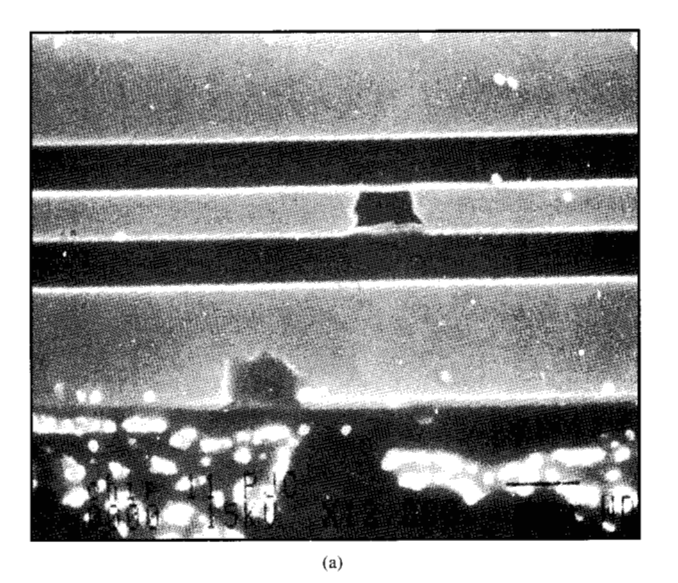
Equation (28b) indicates that plots of  $\Delta R/R$  against  $\sqrt{t}$  should produce straight lines. Furthermore, if  $N_{\rm v}$  is known, we should be able to extract D from the slope of the curves obtained.

Figure 24 shows the fractional resistance change vs. time for an 0.40- $\mu$ m-wide, 0.35- $\mu$ m-thick, 800- $\mu$ m-long Al(0.5 wt.% Cu, 1 wt.% Si) line (double-reservoir) having a redundant underlayer during 2940 h of aging at 225°C (symbols), and the best fit to the data (curve) using Equation (27). For this fit,  $\varepsilon_0 = \alpha \Delta T$ ,  $\alpha_{\rm Al} = 25$  ppm,  $N_{\rm v} = 1$  (only a single void was found by SEM to be contributing

to the resistance change),  $\rho_{\rm A}=3~\mu\Omega$ -cm,  $\rho_{\rm R}=30~\mu\Omega$ -cm, and  $t_{\rm R}=0.07~\mu{\rm m}$ . The net resistance of the redundant layer, which may differ from its bulk value, is found from comparison of the resistance shift for a specific line to the actual area of the voided line, as observed by SEM (e.g., via the SEMs of Figure 25). As is evident from Figure 24, the fit is quite good. A value for the diffusivity can be extracted from the fit, and is found to be  $1.35\times10^{-11}~{\rm cm}^2/{\rm s}$ .

Although the curve fits the data in Figure 24, agreement is not so good as the line width increases. Figure 26 shows plots of  $\Delta R/R_0$  vs.  $\sqrt{t}$  for the same aging time (2940 h,  $\sqrt{t} \approx 55 \text{ h}^{1/2}$ ) for lines having four different widths, w = 0.36, 0.40, 0.48, and  $0.72 \ \mu\text{m}$ . For all cases  $L_0 = 800 \ \mu\text{m}$  and  $t_A = 0.35 \ \mu\text{m}$ ; and several lines were measured for each plot. Two discrepancies were evident. First, the magnitude of the resistance change increased with line width, which was unexpected, and second, the curves generally were not straight lines, as predicted by Equation (28b).

The natural inference to be drawn from the increasing resistance change with increasing line width is that void growth is more rapid for the wider lines. This could be the case if the grain size were small enough, with grain size distribution broad enough that a significant percentage of a line was formed of polycrystalline grains. But the median grain size for these films was about 0.52  $\mu$ m, and their grain sizes were log-normally distributed with a spread of about 0.54. With such a distribution, the frequency of nonbamboo grains in the lines with widths below 0.5  $\mu$ m was quite low, making this explanation untenable. Another possibility was that more voids nucleated and contributed to the resistance change in the wider lines, as was anticipated in developing Equation (28b). To check this latter alternative, lines with four different widths  $(0.36, 0.40, 0.48, 0.72 \mu m)$  with known resistance changes were examined by SEM, and their voids measured. The resistance changes obtained are plotted in Figure 27, and the number of voids for each case is indicated. (The data for the 0.4-µm line are identical to those of Figure 24.) Larger resistance changes clearly correlated with the presence of a greater number of voids in the line. Because of void growth during the "incubation" time, three of the curves in Figure 27 were not amenable to curve fitting. However, growth could be simulated by a straight line passing through the origin and tangent to the specific curve of interest. Corresponding diffusivities could be calculated from Equation (28b), using the slope of the tangent line. Values were thus obtained which were very similar for all four cases, as shown in the third column of Table 2. Note that the value for D listed in the table for the 0.4- $\mu$ m-wide line is somewhat greater than that extracted from the fit of the data shown in Figure 24. This difference arose because use was made of the tangent curve method, which



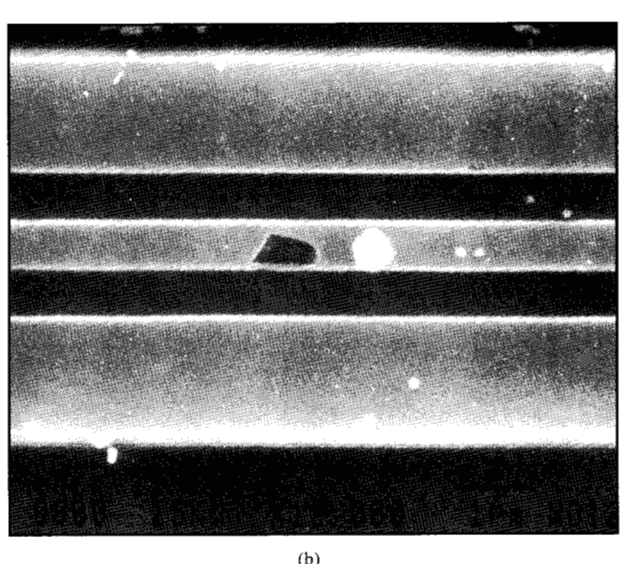
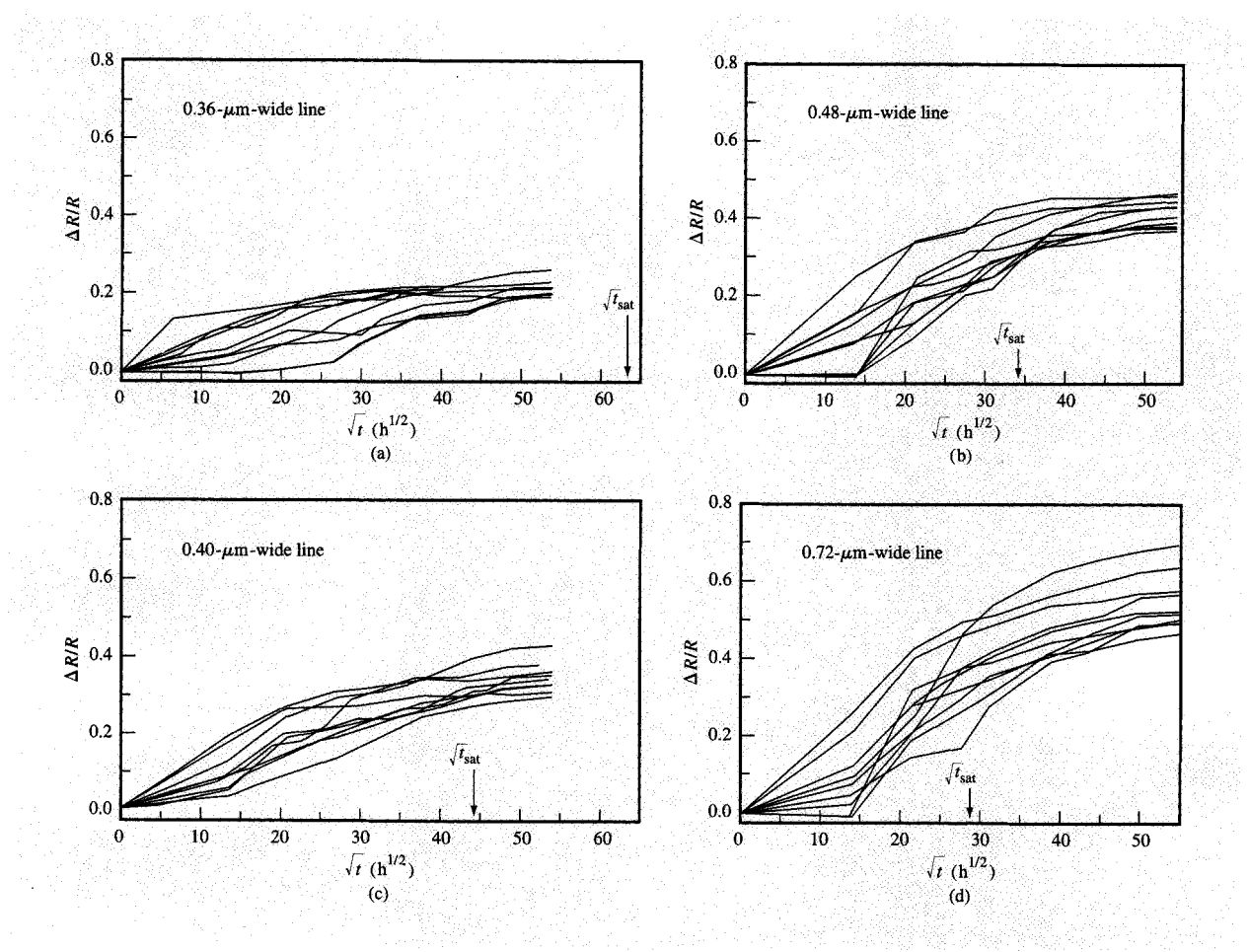


Figure 25

Examples of voids observed via SEM in an 800- $\mu$ m-long, 0.72- $\mu$ m-wide, 0.35- $\mu$ m-thick Al(0.5 wt.% Cu, 1 wt.% Si) line having a redundant underlayer and aged for 750 hours at 225°C: (a) void completely severing the line; (b) void not yet severing the line.

produced a slightly larger slope. Since the 0.4- $\mu$ m-wide line displayed the most well-behaved curve, the diffusivity for that line could be taken as representative for all the line widths. Alternately, the values for all four lines could be averaged. In either case, a value of about  $1.4 \times 10^{-11}$  cm²/s was obtained. We conclude, therefore, that the increase in resistance change with increasing line width is due to the increase in the number of voids rather than an increase in diffusivity with increasing line width.



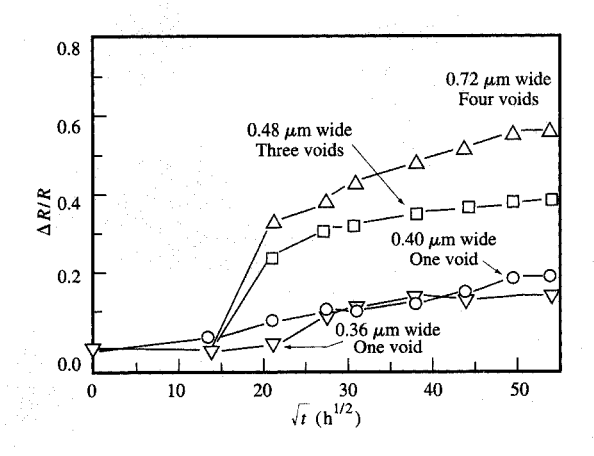
# 1771 (41.2)

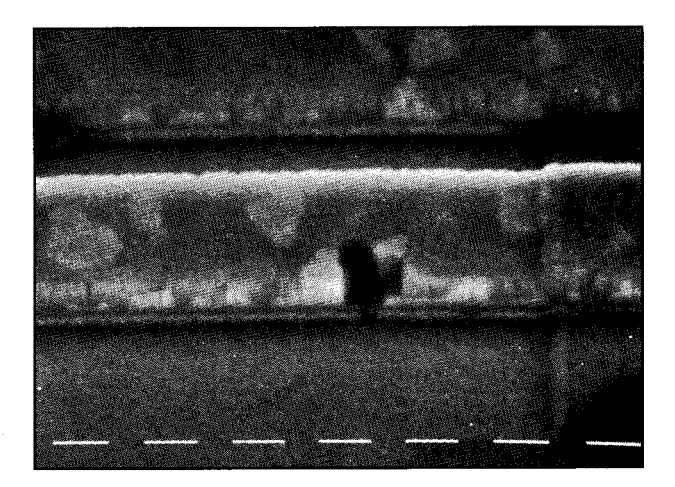
Fractional resistance change vs. square root of time for lines having widths of (a) 0.36, (b) 0.40, (c) 0.48, (d) 0.72  $\mu$ m, aged at 225°C. The arrows on the horizontal axes indicate calculated saturation times based on average void separations.

The dependence of the number of voids on line width deserves some additional comment. Three factors can affect void density: the grain-boundary triple-point density per line length, and Cu precipitate size and distribution. Virtually all SV-related voids are found at grain boundaries, and boundaries are generally accepted to be the nucleation sites for such voids. Since narrower lines contain fewer small grains per unit length, they also have fewer triple-point nucleation sites and fewer voids per length than their wider counterparts. In studies of Al(25 wt.% Cu) films, voids have been observed to form immediately adjacent to the Al, Cu precipitates, leaving them behind (Figure 28). Although this was not investigated at lower Cu concentrations, it probably also occurs down to the 0.5-wt.% range. The precipitates, then, can be assumed not to erode away by diffusion during SV.

Only the Al moves. A total absence of voiding has occasionally been reported in Al(Cu) [57], and is probably due to details of the Cu distribution. Boundary diffusion along a line is apparently completely arrested at such a precipitate in the case of SV. When such precipitates completely block the line, they may limit the size of the reservoir available for void growth, as suggested by the data in Figure 27. As indicated in Figure 10, the density of such blocking precipitates increases with decreasing line width, and probably prevents void growth along large sections of narrow lines. These two factors are also likely to account for much of the variation in void sizes (and associated resistance changes).

Three other aspects of Figure 27 are worth comment. First, both the 0.36- and the 0.40- $\mu$ m-wide lines each contained only one void, yet their resistance-time behavior





Fractional resistance change vs. square root of time for lines having the same widths as for Figure 26.

Figure 2

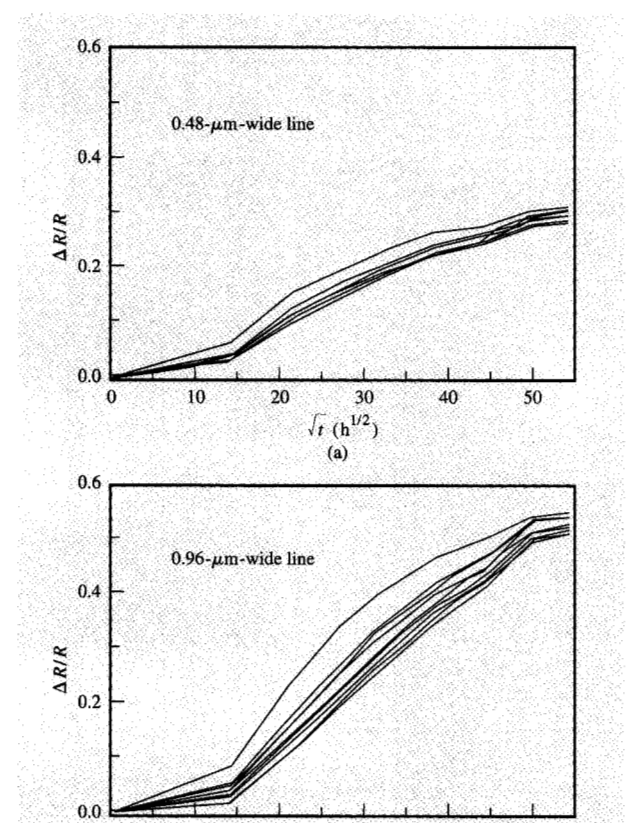
SEM micrograph of voiding in an Al(0.5 wt.% Cu) line. The lighter-contrast grains are Cu precipitates which remain while the surrounding Al diffuses away.

Table 2 Calculated values for voiding at 225°C.

w (μm)	$N_{ar{ extbf{v}}}$	$D(N_{\rm v}) \ ({\rm cm}^2/{\rm s} \times 10^{-11})$	$\overline{N_{_{\mathrm{veff}}}}$	<i>I</i> (μm)	$\frac{\sqrt{t_{\mathrm{sat}}}}{(\sqrt{\mathrm{h}})}$	max ΔR/R	$(\Delta R/R)/N_{_{ m v}}$
0.36	1	1.43	2.23	359	63	0.254	0.114
0.40	1	1.41	3.15	254	44	0.389	0.124
0.48	3	1.55	4.16	192	34	0.468	0.113
0.72	4	1.33	5.10	157	28	0.711	0.139

was different. That for the 0.4-μm-wide line increased in a reasonably linear manner over the entire time period, while that for the 0.36-µm-wide line showed no change through  $\sqrt{t} = 21 \text{ h}^{1/2}$ , then increased rapidly to  $\sqrt{t} = 38 \text{ h}^{1/2}$  and leveled off again. The delay in appearance of a resistance shift and the rapid increase in resistance once a shift was measured were probably effects of void shape. This has not been observed directly, but inferred from observation of voids with irregular shapes which have not yet grown completely across a line (see Figure 25) and produce no measurable resistance shift. The void is believed to grow steadily initially, but without reaching across the line until after attaining a considerable size. This is possible without producing a noticeable resistance change because the Al is 10-20 times more conductive than the redundant layer, and only a small filament of Al(Cu) is needed to keep the resistance low. When the void does finally break through the Al(Cu), the remnants of the final filament diffuse away rapidly, causing the resistance to change swiftly. Thus, void shape effects can produce an "incubation time" in the resistance change as well as abnormally rapid resistance increases.

The second additional aspect of Figure 27 to be noted is the difference in behavior after  $\sqrt{t} = 40 \text{ h}^{1/2}$  between the 0.4-\mu and 0.36-\mu m-wide lines. Whereas resistance of the 0.4-µm-wide line continued to increase, that of the 0.36-um-wide line saturated. With only a single void present in each case, sufficient residual stress existed to drive continued void growth. The unexpected saturation in resistance change for the 0.36-µm line might be explained by the distribution of the Al<sub>2</sub>Cu precipitates. Since, as demonstrated earlier (Figure 10), the density of the blocking Al<sub>2</sub>Cu precipitates increases as the line width narrows, the unexpected saturation in resistance shift may be explainable on the basis of the Al<sub>2</sub>Cu precipitate distribution. Images of both lines were generated by backscattered SEM. Blocking Al, Cu precipitates were observed on either side of the void in the 0.36- $\mu$ m line, separated by 136  $\mu$ m; similar blocking precipitates on either side of the void in the 0.4-µm line were also observed, but these were separated by more than 500 μm, well beyond the volume needed to produce a void of the size observed. Thus, Al<sub>2</sub>Cu precipitate spacing for a given Cu concentration and sufficient



# Figure 29

Fractional resistance change vs. the square root of time for lines 0.48 and 0.96  $\mu$ m wide and 43 cm long. The maximum resistance change is within the expected range, and the behavior is more linear than for 800- $\mu$ m-long lines because of a reduction in line end effects

 $\sqrt{t} \, (h^{1/2})$ 

(b)

small lines appears to be an additional factor which can limit void size.

The third aspect to be noted is the deviation from  $\sqrt{t}$  behavior of the curves for the 0.48- and 0.72- $\mu$ m lines, which manifest a more rapid decrease in the fractional resistance change with time and appear to be approaching zero. This is the behavior expected for void growth saturation. Saturation arises from the depletion of the stress reservoir, and can be caused in long lines by Al<sub>2</sub>Cu precipitate blocking and interactions with nearby voids. Blocking Al<sub>2</sub>Cu precipitates are expected to occur infrequently in the wider lines. Thus, the presence of other voids, which are near enough to drain the stress reservoir, is the more likely cause for saturation. Such effects should begin to appear when  $4\sqrt{Dt/\pi l^2}=1$ , or when

$$t \simeq 0.196 \frac{l^2}{D},\tag{29}$$

where l is the average separation between voids. Average values for the saturation time for the families of curves in Figure 26 can be found once average values for the number of voids have been calculated from average slopes using Equation (28b) and using the diffusivity obtained from measurements of lines containing only one void. Because of the small numbers of voids encountered in the lines, the influence of the line ends must be taken into account. This is done by assuming that voids are present in the wider lines at the line ends, which should increase the calculated value for  $N_{\rm v}$  by 1. The average void separation is then determined by dividing the line length  $L_0=800~\mu{\rm m}$  by  $N_{\rm v}$  (e.g., the void separation for an  $800-\mu{\rm m}$  line with a single void is  $400~\mu{\rm m}$ ).

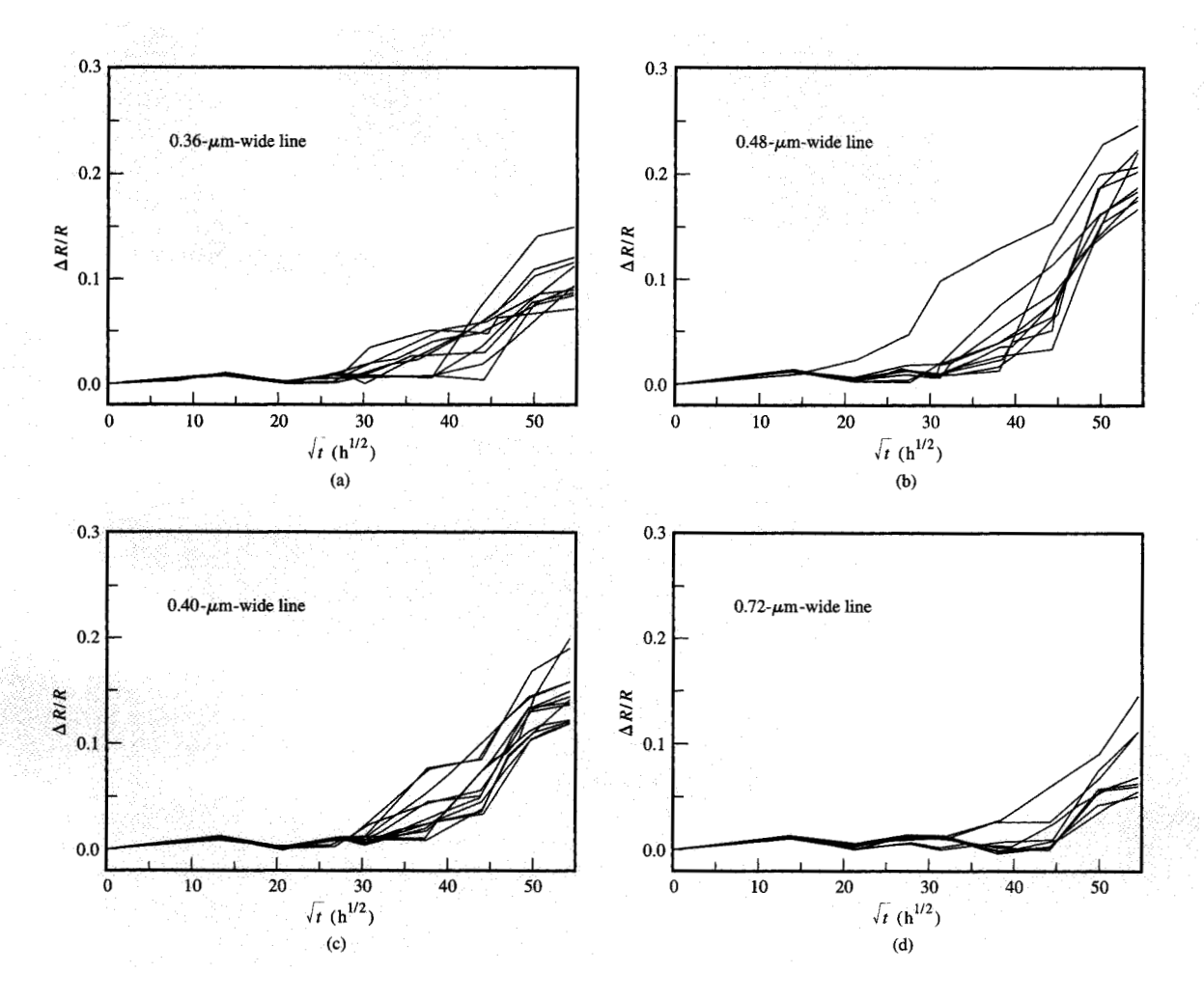
The results of these calculations are also listed in Table 2. Beginning with the fourth column, the effective number of voids, average void separation, and square root of the calculated saturation time are listed. The saturation times are also indicated in Figure 26, and are in reasonable agreement with the locations on the curves at which the average slope changes. Variations can be expected due to differences in void separation and effects due to the Al<sub>2</sub>Cu precipitate spacing. Two additional columns in the table list the maximum fractional resistance shift and this number divided by the calculated number of voids. This value is relatively constant over the four line widths, further strengthening the assertion that differences in measured maximum resistance changes were due to differences in the number of voids present in the lines.

At this point it is useful to calculate the maximum fractional resistance shift expected when all stress in an Al(Cu) line is relieved, i.e., when the void volume approaches  $3\varepsilon_0 V$ , where V is the volume of the line. Assuming that the voids have a rectangular shape, and that all the strain in the Al(Cu) is fully relaxed, the maximum fractional resistance shift is found by letting the total length of voiding,  $L_{voo}$ , be given by

$$L_{v_{\text{tot}}} = N_{v} 3\varepsilon_{0} L_{a} = 3\varepsilon_{0} L_{0} . \tag{30}$$

By using this expression in Equation (26), a value of 0.58 is obtained. Referring to the last two columns of Table 2, we note that the measured values for the 0.72- $\mu$ m-wide line exceeds this by about 20%.

All of the test structures from which data are derived in this section were double-reservoir structures. Thus, the narrow test lines were connected to the outside world through a wider line at each end (as opposed to a W stud), which could act as a reservoir for Al atoms, Cu atoms, and vacancies. Accordingly, the curves which exceeded the theoretical maximum for resistance change were believed



# Finne 30

Fractional resistance change vs. square root of time for lines having widths of (a) 0.36, (b) 0.40, (c) 0.48, (d) 0.72  $\mu$ m. The magnitudes of change are related to the number of voids present in the lines.

to be due to the drawing of vacancies from the reservoirs at the ends. Evidence to support this can be found by comparing the shifts for the 800- $\mu$ m-long lines with those for much longer lines, because the end effects should diminish as the line length increases. The fractional resistance shifts for 0.48- and 1.0- $\mu$ m 43-cm-long lines (**Figure 29**) show that the fractional resistance changes for the lines do not exceed the predicted value of 0.58.

Thus far, we have seen that the most apparent features of the plots in Figure 26 can be explained by a single diffusivity if one takes into account the number of voids present in a line and the effects of Cu precipitates. The apparent change in behavior with line width is an artifact of the increase in the number of voids with increasing line width. Next we examine samples aged at a lower

temperature in order to extract a value for the activation energy for this behavior.

# Temperature dependence

Figure 30 shows the fractional resistance change as a function of the square root of time for lines of Figure 26, but aged at 150°C. It is immediately apparent from the data that the rate of resistance increase had dropped substantially from that shown in Figure 26. First, significant changes evident at 200 h in the 225°C case were not observable until after 900 h at 150°C. Second, the rate of increase was diminished relative to that at 225°C. (Note that the range of the vertical scale in Figure 30 is much smaller than that in Figure 26, making the resistance changes appear larger than they actually are.) The offset in

**Table 3** Calculated values for voiding at 150°C.

w	$\overline{\Delta R/R}_{max}$	$N_{_{ m v}}$ calc.	$D_{_{(150)}}$	$D_{(N_{\mathbf{v}}=1)}$	$N_{_{ m v_d}}$
$(\mu m)$			$(cm^2/s \times 10^{-12})$	$(\mathrm{cm}^2/\mathrm{s}\times 10^{-12})$	
0.36	0.111	1.23	1.37	2.07	1
0.40	0.158	2.15	0.92	4.22	1.5
0.48	0.207	3.16	0.75	7.25	1.9
0.72	0.106	4.10	0.114	1.91	1

time until the first resistance changes were detected was consistent with our hypothesis of the existence of an incubation time for resistance change (similar to that discussed above for electromigration), which is likely a function of void shape. An easily detectable resistance shift occurs only when the Al(Cu) layer becomes discontinuous, and a void can still grow to appreciable size before completely severing the layer. Only when the void is slit-like in shape and extends completely across the line does the shift in resistance track associated void growth. The incubation period is evident in the 225°C data of Figure 26; the data for the  $0.48-\mu m$  and  $0.72-\mu m$ -wide lines display a range of times before the initial resistance increase. Slit-like voids are more apt to occur in narrow lines, bringing the initial resistance change closer to the origin, while rounder voids are more likely to be found in wider lines, causing a shift away from the origin. This trend is exacerbated at 150°C, where even the slit-like voids require some time to totally traverse a line.

A reasonable estimate for the diffusivity at 150°C can still be obtained from the plots by performing an analysis similar to that used above for the 225°C data, except that now an average slope is computed using the average resistance shift at  $\sqrt{t} = 55 \text{ h}^{1/2}$  over the entire aging time in order to account for the incubation time. The results are shown in Table 3. As can be seen from the values listed in the fourth column, the diffusivity appears to decrease from the 0.48- $\mu m$  line to the 0.72- $\mu m$  line, which is not consistent with the behavior observed at 225°C. However, a consistent picture emerges if void shape effects are again considered. At slower growth rates (at lower temperatures), differences in the time required for voids with different shapes to sever the Al(Cu) layer are more clearly resolved in resistance data, and may be separated enough for each void to register separately. Thus, at the initial stage of resistance change, it is entirely reasonable for only a single void to be producing the resistance increase in the 0.72- $\mu m$  line. Nascent voids are probably present in the narrower 0.40- and 0.48-µm lines as well. If the resistance shifts in the 0.36- and 0.72- $\mu$ m lines are assumed to represent the effect of one void, the average numbers of contributing voids per line in the other two lines can be estimated; the estimates are listed in column 6 of Table 3. As can be seen by comparison with column 3, which lists the average number of voids extracted from the 225°C data, fewer voids per line length contribute to the resistance shift at 150°C at the initial stage in the aging process. Since the void nucleation density is not expected to decrease with decreasing temperature, more voids are expected to register with additional aging time.

The diffusivity at 150°C could be obtained from either the 0.36- or 0.72- $\mu$ m-wide line data, and was found to have a value of about  $2 \times 10^{-12}$  cm<sup>2</sup>/s. Figure 31 is a plot of effective diffusivity vs. 1/T. For reference, extrapolated values for both bulk diffusion [42, 86] and grain-boundary diffusion [89] are plotted. For comparison, the estimated values of grain-boundary (dotted line) and interfacial (dashed line) diffusivities of Al extracted from the data in Figure 19 and using  $Z^* = -20$  are also plotted. The activation energy for Al bulk self-diffusion obtained at a temperature >450°C [42] is very close to that of 1.50 eV [43] obtained for Al creep in single crystals of pure Al at temperatures >527°C. They represent samples of commercial purity subjected to stresses at and below the yield stress. A bulk diffusivity with a lower activation energy than that for Al self-diffusion (1.28 eV [86] vs. 1.48 eV [42]) is plotted, as are the values obtained earlier from electromigration studies [91]. By comparison, the values for SV diffusion (solid square points) are quite high. If interpreted in the usual manner, the SV values produce an activation energy of less than 0.5 eV. The preexponential necessary to yield the observed diffusivity is 10<sup>-3</sup> of that for conventional boundary diffusion. A physical system which corresponds to these numbers would have to have a far smaller population of sites for diffusion, and a lower activation energy than would a system of grain boundaries. Of available Al mass transport mechanisms (bulk diffusion, interfacial diffusion, pipe diffusion, grain-boundary diffusion, and vacancy), the most likely candidate for the rapid diffusion observed should be grain-boundary diffusion. However, TEM measurements showed that only small portions of the lines from which the data were obtained were composed of non-bamboo grains, ruling out grain-boundary diffusion. Pipe diffusion could also be ruled out because the dislocation density was far too small to support it, and bulk diffusion is much too

slow to have been considered. Interfacial and vacancy diffusion appeared to be the remaining possibilities. At present, these results are not fully understood. Interpretation of the data was weak, since only two temperatures were used. Unfortunately, the degree of voiding often exhibits variation across individual wafers, as well as from wafer to wafer, suggesting that some as-yet-unidentified processing variable may have been responsible for the rapid diffusion.

The data and analysis we have presented above show that void growth can usually be described by a diffusion model, which can also be used to extract the effective diffusivity for the system being tested. The data indicate that a temperature change from 225°C to 150°C ( $\Delta T = 75$ °C) decreases the diffusivity by an order of magnitude, which represents a rather small amount of acceleration (in comparison with electromigration). Although it is possible to develop an acceleration model based on these data, considerably more work is needed to support it adequately. Until specific mechanisms are better understood, the usefulness of such an acceleration model is limited.

# Refractory layers and product failures

Refractory layers can typically withstand considerable currents without fusing, so that EM tests of Al(Cu) lines with refractory layering result in gradual resistance increases rather than unequivocal open failures. In order to retain the traditional time-to-failure data analysis approach, many workers have used as a failure criterion a resistance increase fraction, e.g., 20%. This approach is unfortunate because it has no connection to actual causes of circuit failure. In addition, variations in design of test structures may inadvertently influence EM evaluations simply by the different time-zero resistance base lines they provide.

Studying these phenomena on double-reservoir structures is extremely difficult, since the influence of damage formation at random nucleation points is brought into play. One traditional approach uses long ( $\gg 1000~\mu m$ ) EM test structures to permit data evaluation in terms of a weakest-link model. The merits of this approach are arguable for simple systems in which failures are decisive, but for layered films in which closed lines are the rule and not the exception, the usefulness of this approach is questionable.

It is preferable to model wiring resistance vs. time as a function of temperature and current. Such a model could, in principle, be used on a circuit-by-circuit basis to set the wiring dimensions needed to limit EM-related failure at an acceptable level, on the basis of the currents the wires carry and the sensitivity of the circuits to resistance changes. Before embarking on this course, which would involve considerable design expense, it is instructive to examine some rough calculations on the relevance of EM-

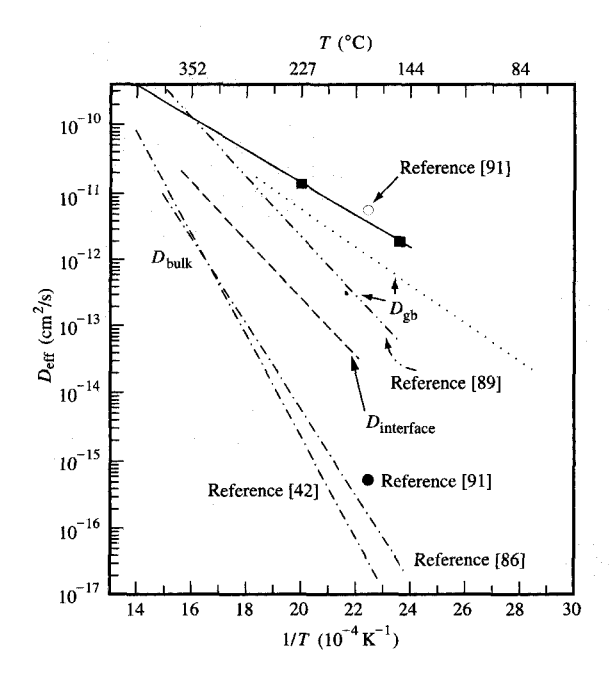


# Figure 31

Effective diffusivity vs. 1/T, showing diffusivity calculated from present SV measurements (straight line and solid squares), compared to grain-boundary diffusivity (8/d) $D_{\rm gb}$  from [89] (dashed-dotted-dotted line); electromigration marker diffusivity (dotted and dashed lines) extracted from Figure 19; and diffusivities (open and closed circles) for multigrained Al(Cu) from [91]. The dashed-dotted lines are extrapolations of bulk diffusivity data from [42] and [86].

related damage to actual circuit reliability. This may help eliminate many possibilities from consideration and thus make EM-related circuit reliability assurance more manageable.

Excluding the power distribution grids, which involve special considerations which are not discussed here, standard CMOS designs may be thought of as networks of pull-up and pull-down devices which charge and discharge capacitive loads. In the present era of 100-MHz designs, performance and power constraints serve to limit most capacitive loads to 1 pF or less. This inherent capacitive load limit is important both for understanding the current-carrying requirements of the interconnection wires and how much resistance degradation circuits can tolerate.

EM stress tests are generally performed at constant currents, whereas circuits operate with current pulses. Fortunately, EM studies with pulsed sources have tended to show that one may equate pulsed EM performance to EM performance at dc for the time-averaged current of the pulses. For a 100% switching factor (i.e., circuit switching every clock cycle)—a worst-case assumption only rarely

applicable to circuits other than clock circuits—the average current for a 1-pF load, 100-MHz clock, and 3.6-V power supply is 0.36 mA (i = fCV). For a 0.7 × 0.7-cross-section interconnection wire, this amounts to a current density of 0.7 mA/ $\mu$ m<sup>2</sup>, which is modest compared to traditional EM design rule current density limits (2–5 mA/ $\mu$ m<sup>2</sup>).

Consider a 50- $\Omega$  resistance increase. This represents approximately a 100% resistance increase for a 800- $\mu$ mlong, single-level EM testing structure with a 0.5- $\mu$ m<sup>2</sup> primary conductor cross-sectional area, i.e., considerably higher than the "failure criterion" usually selected. Such an increase in series with a 1-pF load capacitance causes an *RC* time constant increase of 50 ps. As an isolated event in one stage of a group of circuits with an overall timing requirement of 10 ns, this is usually negligible.

The following argument shows that a  $50-\Omega$  damage site in a CMOS interconnection line is also unlikely to result in refractory fusing causing a catastrophic (open) failure. The occurrence of such fusing at either EM or SV damage sites is determined by the amount of power that can be delivered to the failure point and the effectiveness with which heat can be dissipated from the site. It is important to note that whereas most EM testing involves constant-current sources [and thus unconstrained increases in joule heating  $(i^2R)$  power dissipation] as the resistance due to the damage increases, to first order CMOS circuits are usually constrained to dissipate  $0.5\ CV^2$  energy per transition. As wiring resistance increases in response to EM or SV damage, the location of power dissipation gradually shifts from the transistors to the damage site.

A detailed description of thermal dissipation under various damage scenarios is beyond the scope of this paper. However, the following simplified treatment has been found to give reasonable approximations: The resistance increase a wire experiences as a function of temperature is given by  $R(T, i) = R_0(1 + \alpha \Delta T)$ , where  $R_0$  is the baseline resistance at the temperature  $T_0$ , and  $\alpha = \alpha(T_0)$  is the temperature coefficient of resistance at the baseline temperature. The temperature increase due to joule heating is given by

$$\Delta T = R_{t} P = R_{t} i^{2} R(T, i), \tag{31}$$

where  $R_i$  is the thermal resistance, P the power, and i the current. Combining these equations and rearranging gives

$$1/R(T, i) = 1/R_0 - \alpha R_i i^2. (32)$$

From this equation, R(T, i) is infinite for the "fusing current"  $i_t$ , given by

$$i_{\rm f} = \sqrt{\left(\frac{1}{\alpha} R_{\rm t} R_{\rm 0}\right)}. \tag{33}$$

Assuming that  $R_0 = 50 \Omega$  and using typical values for  $\alpha$  and  $R_0$ , a value of about 10 mA is obtained. Such a value

corresponds to a power dissipation P of 5 mW for a 50- $\Omega$ damage site. For a 100-MHz circuit with a switching factor of 1, this corresponds to a capacitive load of 8 pF  $(P = f \ 0.5 \ CV^2)$ , which is exceptionally high except perhaps for a limited number of off-chip drivers. Note also that the arguments here apply equally well to voids developed by stress voiding and to rms limitations of ac currents which are not expected to generate electromigration degradation directly. This is significant because typically the pulsed dc component of CMOS circuit currents travels in short lines (whose EM-related reliability is probably enhanced by the short-length effects discussed in a previous section) connecting power supply buses through devices to ground, whereas the long across-chip signal lines which connect groups of circuits to one another carry pulsed ac (charge-and-then-discharge) currents.

The preceding arguments imply that only exceptional practical circuits of the present design generation—those with >1-pF loads, high switching factors, and very tight critical timing margins for resistance shift failures, and those with ≥1-pF loads and high switching factors—should fail because of EM according to the EM criteria typically applied. More fundamentally, this shows why a practical knowledge of EM and SV is required in order to predict failure.

A conservative approach to setting EM design rules would be to set a maximum current which would lead to a Cu incubation time corresponding to the desired lifetime of the product at the maximum use temperature and for the worst-case interconnection design. Such a worst-case design would include minimal extra line lengths (reservoirs) at closed ends. In effect, this would mean that the redundancy effects of layering were not being used for EM (but it would still be important for SV and any EM–SV synergy). Projecting the incubation times, for example, for Al(2 wt.% Cu) to  $100^{\circ}$ C,  $3 \text{ mA}/\mu\text{m}^2$  (Figure 15) by using the equation

$$AF = \frac{\tau_{\text{stress}}}{\tau_{\text{use}}} = \exp\left[\frac{Q}{K}\left(\frac{1}{T_{\text{s}}} - \frac{1}{T_{\text{u}}}\right)\right],$$

gives a value of 54 years—a lifetime which should certainly suffice even for this generous current density allowance. Although the application of this approach would require a better understanding of the inherent and systematic variations in incubation time possible across populations of lines, the values cited here are encouraging.

As the technology evolves, operating frequencies are expected to increase, operating voltages are expected to decrease, and typical capacitive loads are expected to decrease. Physical scaling may reduce the redundancy thicknesses, causing voids of a given fractional volume extent to produce increased resistance degradation. These trends make all the more urgent the need for accurate

resistance vs. time models for both EM- and SV-related damage. Finally, it is worth noting that when currents are high enough to make EM a reliability problem, EM is a dominant force compared to SV. Thus, there is some hope that sequential SV and EM testing may result in pessimistic predictions regarding the combined effect actual products experience.

# Concluding remarks

This paper has considered the EM and SV reliability implications of fine Al and Al-alloy lines, with emphasis on the isolated, Al(Cu)-based lines used in IBM VLSI logic and memory chips. Line isolation has potential benefits (e.g., short-line EM and SV suppression) and drawbacks (built-in flux divergences which result in failures much earlier than for double-reservoir lines). Examination of the R(t) behavior of singly closed Al(Cu)-based lines (isolated only at the cathode end) reveals an incubation effect associated with Cu transport followed by Al transport which is sufficient (assuming the presence of a redundant underlayer) not just to form a minimal crack in the primary conductor but to form a void that is substantial enough to cause a significant resistance increase. For long Al(Cu)based lines, resistance changes as a function of current density, test time, and sample temperature can be explained reasonably well by proposed models. Furthermore, links between EM-related failure times and film grain size, texture, precipitate distribution, and morphology can be demonstrated for these long lines. The log-normal distributions of EM-related failure times of isolated, Al(Cu)-based lines tend to display low values of  $\sigma$ (typically 0.2, corresponding to low variability), and an incubation-time behavior which is critical to correctly interpreting accelerated failure data. The incubation-time behavior and apparent interfacial diffusion for EM in isolated, bamboo-grained Al(Cu)-based lines imply that failure times (for a given 1 to 3  $\mu$ m of void growth) of isolated, Al(Cu)-based lines may not necessarily increase drastically as line widths are reduced from multigrained to bamboo-grained dimensions; the interfacial diffusion may be sensitive to the thermally induced stress in the Al(Cu)based lines. The synergy of SV and EM, a complex topic, would need to be examined further in order to more effectively determine its impact on the reliability of such lines.

# **Acknowledgments**

We would like to acknowledge the efforts of our colleagues at the Silicon Facility of the IBM Thomas J. Watson Research Center, Yorktown Heights, NY, and at the IBM Microelectronics Division, Burlington, VT, for film deposition and the fabrication of fine-line samples. We are also grateful to G. A. Biery, J. M. E. Harper, D. B. Knorr, and R. Rosenberg for helpful comments on the

manuscript, to J. L. Hurd for Figures 3 and 4, and to C. Stanis for providing TEM micrographs.

# References

- See for example J. G. Ryan, R. M. Geffken, N. R. Poulin, and J. R. Paraszczak, *IBM J. Res. Develop.* 39, 371 (1995, this issue); and T. J. Licata, E. G. Colgan, J. M. E. Harper, and S. E. Luce, *IBM J. Res. Develop.* 39, 419 (1995, this issue).
- For review articles, see for example P. S. Ho and T. Kwok, Rep. Progr. Phys. 52, 301 (1989); and A. Scorzoni, B. Neri, C. Caprile, and F. Fantini, Mater. Sci. Rep. 7, 143 (1991).
- 3. H. Okabayshi and K. Aizawa, Second International Stress Workshop on Stress Induced Phenomena in Metallization, P. Ho, P. Totta, and C.-Y. Li, Eds., American Institute of Physics, New York, 1994, p. 33.
- See for example D. R. Cote, S. V. Nguyen, W. J. Cote, S. L. Pennington, A. K. Stamper, and D. V. Podlesnik, IBM J. Res. Develop. 39, 437 (1995, this issue).
- H. S. Rathore, R. G. Filippi, R. A. Wachnik, J. J. Estabil, and T. Kowk, Second International Stress Workshop on Stress Induced Phenomena in Metallization, American Institute of Physics, New York, 1994, p. 165.
- F. d'Heurle and P. S. Ho, in *Thin Films: Interdiffusion and Reactions*, J. Poate, K. N. Tu, and J. Mayer, Eds., John Wiley, New York, 1978, Ch. 8.
- 7. H. H. Hoang, R. A. Coy, and J. W. McPherson, Proceedings of the 7th International IEEE VLSI Multilevel Interconnection Conference, 1990, p. 133.
- B. N. Agarwala, M. J. Attardo, and P. Ingraham, J. Appl. Phys. 41, 3954 (1970).
- S. Vaidya, T. T. Sheng, and A. K. Sinha, Appl. Phys. Lett. 36, 464 (1980).
- 10. A. S. Oates, *Proceedings of the IEEE International Reliability Physics Symposium*, 1990, p. 20.
- 11. J. Tao, K. Konard, N. Cheung, and C. Hu, *IEEE Trans. Electron Devices* 40, 1398 (1993).
- 12. S. Vaidya and A. K. Sinha, *Thin Solid Films* **75**, 253 (1981).
- 13. D. B. Knorr, *Mater. Res. Soc. Symp. Proc.* **309**, 127 (1903)
- 14. E. G. Colgan and K. P. Rodbell, *J. Appl. Phys.* **75**, 3423 (1994)
- B. R. Livesay, N. E. Donlin, A. K. Garrison, H. M. Harris, and J. L. Hubbard, *Proceedings of the 30th International Reliability Physics Symposium*, 1992, p. 217.
- A. Ohsaki, K. Maekawa, Y. Kohgo, J. Komori, Y. Itoh, and H. Kotani, Conference Proceedings, Murray Hill, NJ, and Tokyo, Japan, October 8-10, 1991; Materials Research Society, Pittsburgh, 1992, p. 335.
- 17. A. K. Rajagopal and S. Teitler, *IEEE Trans. Reliabil.* 39, 110 (1990).
- D. P. Bouldin, Tutorials, in Proceedings of the 11th International VLSI Multilevel Interconnection Conference, 1994, p. 266.
- T. A. Oates, E. P. Martin, D. Alugbin, and F. Nkansah, *Appl. Phys. Lett.* 62, 3273 (1993).
- C. K. Hu, P. S. Ho, and M. B. Small, J. Appl. Phys. 72, 291 (1992).
- 21. I. A. Blech, J. Appl. Phys. 47, 1203 (1976).
- 22. J. A. Thornton, J. Vac. Sci. Technol. A 4, 3059 (1986).
- 23. J. Cho and C. V. Thompson, *Appl. Phys. Lett.* **54**, 2577 (1989).
- D. T. Walton, H. J. Frost, and C. V. Thompson, *Appl. Phys. Lett.* 61, 40 (1992).
- C.-K. Hu, M. B. Small, K. P. Rodbell, N. Mazzeo, P. Blauner, R. Rosenberg, and P. S. Ho, *Mater. Res. Soc. Symp. Proc.* 309, 111 (1993).

- C.-K. Hu, N. Mazzeo, and C. Stanis, *Mater. Chem. Phys.* 35, 95 (1993).
- M. L. Dreyer and C. J. Varker, Appl. Phys. Lett. 60, 1860 (1992).
- 28. E. Arzt and W. D. Nix, J. Mater. Res. 6, 731 (1991).
- D. B. Knorr, "Textures in Thin Films," Proceedings of the International Conference on Textures of Materials, ICOTOM, 1994, p. 10.
- D. P. Tracy, D. B. Knorr, and K. P. Rodbell, J. Appl. Phys. 76, 2671 (1994).
- 31. D. B. Knorr, D. P. Tracy, and K. P. Rodbell, *Appl. Phys. Lett.* **59**, 3241 (1991).
- 32. A. Campbell, R. E. Mikawa, and D. B. Knorr, *J. Electron. Mater.* 22, 589 (1993).
- K. P. Rodbell, D. B. Knorr, and J. D. Mis, J. Electron. Mater. 22, 597 (1993).
- J. L. Hurd, K. P. Rodbell, D. B. Knorr, and N. L. Koligman, *Mater. Res. Soc. Symp. Proc.* 343, 653 (1994).
- C. J. Simpson, K. T. Aust, and W. C. Winegard, *Metall. Trans.* 2, 987 (1971).
- A. D. Rollett, D. J. Srolovitz, and M. P. Anderson, *Acta Metall.* 37, 1227 (1989).
- H. B. Huntington, in *Diffusion in Solids: Recent Developments*, A. S. Nowick and J. J. Burton, Eds., Academic Press, Inc., New York, 1974, Ch. 4.
- 38. I. Kaur and W. Gust, *Handbook of Grain and Interphase Boundary Diffusion Data*, Ziegler Press, Stuttgart, 1989, Vol. 1, pp. 118-123.
- C.-K. Hu, P. S. Ho, and M. B. Small, J. Appl. Phys. 74, 969 (1993).
- 40. R. W. Balluffi, Phys. Stat. Sol. 42, 11 (1970).
- C. K. Hu, R. Rosenberg, and K. N. Tu, Proceedings of the Second International Stress Workshop on Stress Induced Phenomena in Metallization, P. Ho, P. Totta, and C.-Y. Li, Eds., American Institute of Physics, New York, 1994, p. 195.
- 42. T. S. Lundy and J. F. Murdock, J. Appl. Phys. 33, 1671 (1962).
- 43. J. L. Lytton, L. A. Shepard, and J. E. Dorn, *Trans. AIME* 212, 220 (1958).
- 44. T. D. Sullivan, Appl. Phys. Lett. 55, 2399 (1989).
- R. G. Filippi, G. A. Biery, and M. Wood, *Mater. Res. Soc. Symp. Proc.* 309, 141 (1993).
- J. J. Estabil, H. R. Rathore, and E. N. Levine, Proceedings of the 8th International IEEE VLSI Multilevel Interconnection Conference, 1991, p. 242.
- 47. M. J. Attardo and R. Rosenberg, *J. Appl. Phys.* 41, 2381 (1970).
- 48. K. P. Rodbell, P. W. DeHaven, and J. D. Mis, *Mater. Res. Soc. Symp. Proc.* 225, 91 (1991).
- C. C. Lee, E. S. Machlin, and H. Rathore, J. Appl. Phys. 71, 5877 (1992).
- 50. I. A. Blech, J. Appl. Phys. 47, 1203 (1976).
- C. A. Ross, J. S. Drewery, R. E. Somekh, and J. E. Evetts, *J. Electron. Mater.* 19, 911 (1990).
- 52. F. M. d'Heurle and R. Rosenberg, *Phys. Thin Solid Films* 7, 257 (1973).
- 53. I. Ames, F. M. d'Heurle, and R. E. Horstmann, *IBM J. Res. Develop.* **14**, 461 (1970).
- 54. R. Rosenberg, J. Vac. Sci. Technol. 9, 263 (1972).
- C. K. Hu, P. S. Ho, M. B. Small, and K. Kelleher, Mater. Res. Soc. Symp. Proc. 225, 99 (1991).
- S. E. Rauch and T. D. Sullivan, in Submicron Metallization: Challenges, Opportunities and Limitations, International Society for Optical Engineering (SPIE), Bellingham, WA, 1992, Vol. 1805, p. 197.
- J. G. Ryan, J. B. Riendeau, S. E. Shore, G. J. Slusser,
   D. C. Beyar, D. P. Bouldin, and T. D. Sullivan, J. Vac. Sci. Technol. A 3, 1474 (1990).
- S. Mayumi, T. Umemoto, M. Shishino, H. Nanatsue,
   S. Ueda, and M. Inoue, Proceedings of the 25th International Reliability Physics Symposium, 1987, p. 15.

- J. Onuki, Y. Koubuchi, S. Fukada, M. Suwa, Y. Misawa, and T. Itagaki, *IEDM Tech. Digest*, p. 454 (1988).
- J. Onuki, Y. Koubuchi, M. Suwa, M. Koizumi, D. S. Garder, H. Suzuki, and E. Minowa, *IEEE Trans. Electron Devices* 39, 1322 (1992).
- A. G. Dirks and R. A. Augur, Appl. Phys. Lett. 64, 704 (1994).
- J. Ogawa and H. Nishimura, *IEDM Tech. Digest*, p. 277 (1991).
- 63. T. Hara, N. Hosoda, S. Nagano, and T. Ueda, *Jpn. J. Appl. Phys.* **32**, 1395 (1993).
- T. J. Licata, T. D. Sullivan, R. C. Bass, J. G. Ryan, and D. B. Knorr, *Mater. Res. Soc. Symp. Proc.* 309, 87 (1993).
- R. M. Geffken, J. G. Ryan, and G. J. Slusser, *IBM J. Res. Develop.* 31, 608 (1987).
- J. K. Howard, J. F. White, and P. S. Ho, J. Appl. Phys. 49, 4083 (1978).
- 67. D. S. Gardner, T. L. Michalka, K. C. Saraswat, T. W. Barbee, J. P. McVittie, and J. D. Meindl, *IEEE Trans. Electron Devices* ED-32, 174 (1985).
- G. J. Slusser, J. G. Ryan, S. E. Shore, M. A. Lavoie, and T. D. Sullivan, J. Vac. Sci. Technol. A 7, 1568 (1989).
- H. Shibata, M. Murota, and K. Hashimoto, *Jpn. J. Appl. Phys.* 32, 4479 (1993).
- D. Jawarani, J. P. Stark, H. Kawasaki, J. O. Olowolafe, C. C. Lee, J. Klein, and F. Pintchovski, J. Electrochem. Soc. 141, 302 (1994).
- K. P. Rodbell, E. G. Colgan, and C. K. Hu, *Mater. Res. Soc. Symp. Proc.* 337, 59 (1994).
- L. F. Mondolfo, Aluminum Alloys: Structure and Properties, Butterworths Publishers, London, 1976, p. 254.
- D. R. Frear, J. E. Sanchez, A. D. Romig, and J. W. Morris, Jr., *Metall. Trans.* 21A, 2449 (1990).
- 74. C. Kim and J. W. Morris, Jr., *J. Appl. Phys.* **73**, 4885 (1993).
- C.-K. Hu, M. B. Small, K. Rodbell, C. Stanis, P. Blauner, and P. S. Ho, *Appl. Phys. Lett.* 62, 1023 (1993).
- 76. C.-K. Hu, Thin Solid Films 260, 124 (1995).
- 77. H. P. Longworth and C. V. Thompson, *Mater. Res. Soc. Symp. Proc.* **265**, 95 (1992).
- R. W. Vook, C. Y. Chang, and C. W. Park, *Proc. SPIE* 1805, 232 (1993).
- 79. R. W. Vook and C. Y. Chang, Appl. Surf. Sci. 60, 71 (1992)
- D. Gupta, K. Vieregge, K. P. Rodbell, and K. N. Tu, Proceedings of the Symposium on Diffusion in Ordered Alloys and Intermetallic Compounds, B. Fultz, R. Cahn, and D. Gupta, Eds., TMS, Warrend, PA, 1992, p. 247.
- 81. N. L. Peterson and S. J. Rothman, *Phys. Rev. B* 1, 3264 (1970).
- 82. P. S. Ho and H. K. Howard, Appl. Phys. Lett. 27, 261 (1975).
- 83. I. A. Blech, J. Appl. Phys. 48, 473 (1977).
- 84. A. S. Oates and D. L. Barr, J. Electron. Mater. 23, 63 (1994).
- 85. H.-U. Schreiber, Solid-State Electron. 29, 893 (1986).
- A. Seeger, D. Wolf, and H. Mehrer, *Phys. Status Solidi B* 48, 481 (1971).
- 87. J. Curry, G. Fitzgibbon, Y. Guan, R. Muollo, G. Nelson, and A. Thomas, *Proceedings of the 22nd International Reliability Physics Symposium*, 1984, p. 6.
- 88. H. Okabayashi, Mater. Sci. Eng. R11, 191 (1993).
- 89. H. J. Frost and M. F. Ashby, *Deformation-Mechanism Maps*, Pergamon Press, New York, 1982, p. 21.
- F. R. N. Nabarro, in Report on a Conference on the Strength of Solids, Physical Society, London, 1948, p. 75.
- 91. F. M. d'Heurle and A. Gangulee, in *The Nature and Behavior of Grain Boundaries*, H. Hu, Ed., Plenum Press, New York, 1972, p. 339.

Received December 9, 1994; accepted for publication April 19, 1995

Chao-Kun Hu IBM Research Division, Thomas J. Watson Research Center, P.O. Box 218, Yorktown Heights, New York 10598. (CKHU at YKTVMV, ckhu@watson.ibm.com). Dr. Hu is a research staff member in the Silicon Technology Department at the IBM Thomas J. Watson Research Center. He obtained a B.S. degree from Chung Yuan College, and an M.S. degree from the Institute of Physics, National Tsing Hua University, Taiwan. Dr. Hu received his Ph.D. degree in physics from Brandeis University in 1979. He was a research associate at Rensselaer Polytechnic Institute before joining IBM in 1984. Dr. Hu's current research is in the area of electromigration reliability of on-chip interconnections. He is a member of the American Vacuum Society.

Kenneth P. Rodbell IBM Research Division, Thomas J. Watson Research Center, P.O. Box 218, Yorktown Heights, New York 10598 (RODBELL at YKTVMV, rodbell@watson.ibm.com). Dr. Rodbell is a research staff member in the Thin Film Metallurgy and Interconnection Department at the IBM Thomas J. Watson Research Center. In 1982, 1983, and 1986, respectively, he received B.S., M.S., and Ph.D. degrees in materials engineering from Rensselaer Polytechnic Institute, where he was supported by an IBM Graduate Fellowship. He joined IBM in 1986 and spent three years at the IBM Semiconductor Development Laboratory in Hopewell Junction, New York, moving to IBM Research in 1989. Dr. Rodbell's technical interests include thin-film microstructural evolution, crystallographic texture, alloy development, interdiffusion, 1/f noise, and reliability. He is a member of the Materials Research Society.

Timothy D. Sullivan IBM Microelectronics Division, Burlington facility, Essex Junction, Vermont 05452 (TSULLIV at BTVLABVM, tsulliv@btvlabvm.vnet.ibm.com). Dr. Sullivan is an advisory scientist in technology reliability engineering at the IBM facility in Essex Junction, Vermont. He joined IBM in 1984; since then, his responsibilities have included qualification of new technologies, measurement and modeling of chip interconnect failure mechanisms, especially stress-induced voiding in Al-based metallizations, and electromigration. Dr. Sullivan received a B.A. degree in physics in 1971 from Northeastern University, and M.S. and Ph.D. degrees in materials science in 1982 and 1985, respectively, from Cornell University. He is a member of the Materials Research Society.

Kim Y. Lee IBM Microelectronics Division, Thomas J. Watson Research Center, P.O. Box 218, Yorktown Heights, New York 10598 (KYL at YKTVMV, kyl@watson.ibm.com). Dr. Lee is an advisory engineer in the Interconnection Materials and Modeling Department at the IBM Thomas J. Watson Research Center. He received his B.Sc. and Ph.D. degrees in electrical and electronics engineering from the University of Glasgow, United Kingdom, in 1983 and 1987, respectively. Dr. Lee subsequently joined IBM at the Thomas J. Watson Research Center, where, as a Visiting Scientist, he worked on nanostructure fabrication. In 1990 he received an IBM Outstanding Technical Achievement Award for his work on zero-dimensional structures. In 1990, Dr. Lee joined the IBM Microelectronics Division; he is currently working on sub-0.25-µm interconnects.

Dennis P. Bouldin IBM Microelectronics Division, Burlington facility, Essex Junction, Vermont 05452 (DBOULDI at BTVVMOFS, DBOULDI@btvlabvm.vnet.ibm.com). Dr. Bouldin is a senior scientist/engineer at the IBM facility in Essex Junction, Vermont. He is currently the manager of a logic interconnect process development group. Until March 1995, he was a technical team leader in a technology reliability group. This involved the coordination of interconnect technology reliability engineering activities among programs at the Essex Junction facility, the IBM Semiconductor Research facility in Hopewell Junction, New York, and the Thomas J. Watson Research Center in Yorktown Heights, New York. It also involved the development of advanced interconnect reliability characterization and implementation methods, and encompassed technologies in manufacturing or development ranging from 4Mb to 256Mb DRAMs and 2-μm-4-μm CMOS logic circuits. Dr. Bouldin's previous assignments at IBM have included work in materials analysis and characterization and in engineering computation. He received a Ph.D. in physics from Brown University and an undergraduate degree in physics from Rice University.